

Testing strong gravitational lensing effects of supermassive compact objects with regular spacetimes

JITENDRA KUMAR,¹ SHAFQAT UL ISLAM,¹ AND SUSHANT G. GHOSH^{2,1}

¹ *Centre for Theoretical Physics, Jamia Millia Islamia, New Delhi 110025, India*

² *Astrophysics Research Centre, School of Mathematics, Statistics and Computer Science, University of KwaZulu-Natal, Private Bag 54001, Durban 4000, South Africa*

ABSTRACT

We compare and contrast gravitational lensing, in the strong field limit, by the photon sphere in spherically symmetric regular electrically charged (REC) black holes ($0 < b \leq b_E$) and with those by corresponding REC no-horizon spacetimes ($b > b_E$). Here, b is an additional parameter due to the charge and the value $b = b_E \approx 0.226$ corresponds to an extremal black hole with degenerate horizons. Interestingly, the spacetime admits a photon sphere for $0 < b \leq b_P \approx 0.247$ and an anti-photon sphere only for $b_E < b \leq b_P$. With no-horizon spacetime, images by lensing from the inside of the photon sphere ($u < u_{ps}$) can also appear. Interestingly, for the case of $u < u_{ps}$ the deflection angle α_D increases with u . We analyse the lensing observables by modeling compact objects Sgr A*, M87*, NGC 4649, and NGC 1332 as black holes and no-horizon spacetimes. The angular position θ_∞ and photon sphere radius x_{ps} decrease with increasing parameter b . Our findings suggest that the angular separations (s) and magnification (r) of relativistic images inside the photon sphere may be higher than those outside. Moreover, the time delay for Sgr A* and M87* can reach ~ 8.8809 and ~ 12701.8 minutes, respectively, at $b = 0.2$, deviating from Schwarzschild black holes by ~ 2.615 and ~ 4677 minutes. These deviations are insignificant for Sgr A* because it is too small, but they are sufficient for astronomical observation of M87* and some other black holes. With EHT bounds on the θ_{sh} of Sgr A* and M87*, within the 1σ region, placing bounds on the parameter b , our analysis concludes that the REC black holes agree with the EHT results in finite space, whereas the corresponding REC no-horizon spacetimes are completely ruled out.

Keywords: Galaxy: center– gravitation – black hole physics -black hole shadow- gravitational lensing: strong

1. INTRODUCTION

The weak cosmic censorship conjecture (CCC) by Penrose (1969), found that there can be no singularity visible from future null infinity, i.e., light rays originating from singularity are entirely blocked by the event horizon. Whereas the strong CCC prohibits its visibility by any observer. That means no light rays emanate out of the singularity, i.e., it is never naked, which mathematically precisely means spacetime should be globally hyperbolic. Despite almost half a decade of effort, we are still far from a general proof of CCC (for recent reviews and counterexamples, see (Joshi 1993; Wald 1997; Singh 1999; Clarke 1994; Harada 2004; Joshi 2012)). The gravitational lensing

shows excellent potential for distinguishing black holes from naked singularities based on qualitatively different lensing features (Virbhadrha & Ellis 2002; Virbhadrha 1996, 1999; Virbhadrha & Keeton 2008) introducing the question as to whether CCC could be tested observationally. Gravitational lensing is a meaningful astronomical means as it provides information about sources and lenses and the large-scale geometry of the universe.

The idea of gravitational lensing was pioneered by Darwin (1959), who investigated photon trajectories passing in the environs of a black hole and showing the more significant deflection of a light ray, which in turn, guided an exact lens equation (Frittelli et al. 2000; Virbhadrha & Ellis 2000). Later, Virbhadrha et al. (1998), and Virbhadrha and Ellis (2000) conducted a numerical investigation of lensing by static, spherically symmetric naked singularity and scrutinized lensing

observables. Motivated by this, Perlick (2004) probed lensing in a spherically symmetric and static spacetime based on the light-like geodesic equation without approximations. It turns out that lensing by black holes is an excellent astrophysical tool for investigating gravity’s strong field features and providing information about the faraway dim stars.

Due to its importance, the gravitational lensing by various black holes has attracted much attention in the past few decades with the functional, analytical techniques of Bozza (2001) based on the strong deflection of the light ray, showing that the deflection angle diverges logarithmically as light rays come to the photon sphere of a Schwarzschild black hole. The Bozza’s recipe was applied to Reissner-Nordström black holes (Eiroa et al. 2002), and also to an arbitrary static, spherically symmetric metric (Bozza 2002). One of the motivations behind the diverse works on gravitational lensing is that the trajectories of light near black holes are related to the background geometry’s essential features and properties, and also the anticipation that the relativistic images should test the gravity in the strong deflection limit led to applying this technique to diverse black hole metrics from general relativity and modified theories (Fernando & Roberts 2002; Bozza 2003; Majumdar & Mukherjee 2005; Eiroa & Romero 2008; Bozza 2015; Sahu et al. 2015; Islam & Ghosh 2021). Moreover, significant attention has been devoted to gravitational lensing by naked singularities or no-horizon spacetimes (Gyulchev & Yazadjiev 2007). The quantitative features of gravitational lensing can distinguish horizonless compact objects from black holes (Gyulchev & Yazadjiev 2007, 2008). Recently, Shaikh *et al.* (2019) performed an analytical investigation of strong gravitation lensing from such horizonless compact objects to obtain exact expressions of lensing observables for the images formed by lensing from the inside of the photon sphere and compared them with those formed from the outside.

This paper aims to investigate gravitational lensing by a class of spherical symmetric regular electrically charged (REC) black hole spacetimes (Dymnikova 2004), and probe how it differs from lensing by the corresponding no-horizon spacetimes. Assuming the supermassive black holes Sgr A* and M87* as the lens, we also compare REC black holes’ observable signatures with those of the Schwarzschild black holes. Interestingly, although it is feasible to detect some effects of the strong deflection lensing by the REC black holes with the Event Horizon Telescope (EHT) observations, it is tricky to distinguish two black holes

as deviations are $\mathcal{O}(\mu\text{as})$. We also use the EHT results from M87* and Sgr A* black hole shadow to constrain the deviation from the Kerr black hole and to assess the viability of REC regular black holes and no-horizon spacetimes. By its very definition, the existence of a singularity means spacetime fails to exist, signaling a breakdown of the laws of physics. In the absence of a well-developed definite quantum gravity permitting us to obtain the interior of the black hole and resolve it separately (Wheeler 1963), one must turn their attention to regular models, which are inspired by quantum assertions. The earliest idea by Sakharov (1966) and Gliner (1966) proposes that singularities could be avoided by matter with a de Sitter core, which could provide good discrimination at the final stage of gravitational collapse, replacing the future singularity (Gliner 1966). Based on this idea, Bardeen (1968) provided the first regular black hole solution (Bardeen 1968) with horizons, but with no central singularity. There has been a significant amount of attention paid to the analysis and application of regular black holes (Dymnikova 1992; Ayon-Beato & Garcia 1998, 1999; Bronnikov 2000, 2001; Burinskii & Hildebrandt 2002; Dymnikova 2004; Hayward 2006; Bronnikov & Fabris 2006; Hayward 2006; Zaslavskii 2009; Lemos & Zanchin 2011; Junior et al. 2015; Fan & Wang 2016; Bronnikov 2017; Sajadi & Riazi 2017; Toshmatov et al. 2018). It has an additional parameter g because of a magnetic monopole charge (Ayon-Beato & Garcia 1998), apart from mass M and encompasses the Schwarzschild metric as a particular case ($g = 0$). Thus, the black hole interior does not result in a singularity but develops a de Sitter-like region, eventually settling with a regular center: thus, its maximal extension is one of a Reissner–Nordström spacetime but with a regular center (Borde 1994, 1997). Also a significant amount of attention has been devoted to finding an extension, and uncovering of the properties of Bardeen black holes has been reported (Ansoldi 2008; Lemos & Zanchin 2011; Sharif & Javed 2011; Fernando & Correa 2012; Flachi & Lemos 2013; Bambi 2014; Ulhoa 2014; Ghosh & Amir 2015; Schee & Stuchlik 2015; Breton & Lopez 2016; Saleh et al. 2018; Ali & Ghosh 2019; Dey & Chakrabarti 2019; Toshmatov et al. 2019; Kumar et al. 2020b; Ghosh et al. 2020; Kumar et al. 2020a, 2022a; Islam et al. 2022), and also in higher dimensional spacetimes (Ali & Ghosh 2018; Kumar et al. 2019; Singh et al. 2020). Interestingly, the Bardeen model may also be interpreted as a solutions of Einstein equations with an electric source (Rodrigues & Silva 2018). Dymnikova (2004) proved

the existence of electrically charged structures with a regular center, in which geometry, field, and stress-energy tensor are regular.

There is a good amount of motivation to constrain the electric charge of black holes, which has seen a multitude of efforts in this direction (Takahashi 2005; Kocherlakota et al. 2021; Akiyama et al. 2022a). The charge of Sgr A* has also been constrained to be $Q \leq 3.1 \times 10^8 C$ using Chandra X-ray data (Karouzos 2018; Zajaček et al. 2018). We intend to see whether we can improve this by using electromagnetic observations of supermassive black holes with the EHT results. The authors (Kumar & Ghosh 2020; Ghosh et al. 2021; Kumar Walia et al. 2022) demonstrated that the charged rotating regular black holes and corresponding no-horizon spacetimes agree with the EHT observations. Thus, charged rotating regular spacetimes and Kerr black holes are indiscernible in some parameter space, and one cannot rule out the possibility of the former being strong candidates for astrophysical black holes. A contribution to the characteristic lensing quantities because of the higher-order terms, viz., the gravitomagnetic terms considered in the lens potential, is analyzed. It turns out that gravitomagnetic effects originate from the mass current in the lens and under some circumstances could give rise to results that could be detected with future observations (Capozziello & Re 2001; Capozziello et al. 1999). It is because of the Rytov effect, i.e., the change in electromagnetic wave polarization in a smoothly inhomogeneous isotropic medium in a geometrical optics approximation (Rytov 1938).

Therefore, it would be fascinating to explore the gravitation lensing by REC black holes/no-horizon spacetimes and compare it with a Schwarzschild black hole to place constraints on the deviation parameter.

This paper is organized as follows: In the Sec. 2, the spacetime structure of the REC black hole is briefly reviewed for completeness with a special focus on the energy conditions. The setup for gravitational lensing, including the lens equation, deflection angle, and the strong lensing coefficients, is given in Sec. 3. The strong lensing observables, i.e., the apparent size of the photon sphere (position of innermost image), the separation between the images and the difference in the brightness between the relativistic images are also part of Sec. 3. Time delay for supermassive black holes Sgr A*, M87*, and those at the centres of 21 other galaxies have been estimated in Sec. 4. Sec. 5 is dedicated to the no-horizon spacetime wherein we discuss the lensing just inside the photon sphere and

calculate the lensing observables in this case. The lensing observables for Sgr A*, M87*, NGC 4649, and NGC 1332 are discussed in Sec. 6. In Sec. 7, we derive constraints on the rotating REC black hole parameter b with the aid of EHT results from M87* and Sgr A* black hole shadow. We summarize our results and conclude the paper in Sec. 8.

We have used units that fix the speed of light and the gravitational constant $8\pi G = c = 1$, but they are restored in the tables.

2. REC SPACETIMES

Here, we start with the action of gravity, minimally coupled to nonlinear electrodynamics, given by

$$S = \frac{1}{16\pi} \int d^4x \sqrt{-g} (R - \mathcal{L}(F)); \quad F = F_{\mu\nu} F^{\mu\nu}, \quad (1)$$

which contains Ricci scalar R , and $F_{\mu\nu} = \partial_\mu A_\nu - \partial_\nu A_\mu$ is the electromagnetic field. The gauge-invariant electromagnetic Lagrangian $\mathcal{L}(F)$ is an arbitrary function of F , which in the weak field regime, should have the Maxwell limit, $\mathcal{L} \rightarrow F$, $\mathcal{L}_F \rightarrow 1$.

Action (1) gives the dynamic field equations

$$\nabla_\mu (\mathcal{L}_F F^{\mu\nu}); \quad \nabla_\mu (*F^{\mu\nu}) = 0, \quad (2)$$

where $\mathcal{L}_F = d\mathcal{L}/dF$. In the spherically symmetric case, the only nonzero components of $F_{\mu\nu}$ are a radial electric field $F_{01} = -F_{10} = E(r)$ and a radial magnetic field $F_{23} = -F_{32}$. The Einstein equations take the form (Bronnikov 2001)

$$G_\nu^\mu = -T_\nu^\mu = 2\mathcal{L}_F F_{\nu\alpha} F^{\mu\alpha} - \frac{1}{2} \delta_\nu^\mu \mathcal{L}. \quad (3)$$

The density and pressures for electrically charged source are given by

$$\rho = -p_r = \frac{1}{2} \mathcal{L} - F \mathcal{L}_F; \quad p_\perp = -\frac{1}{2} \mathcal{L}, \quad (4)$$

and the scalar curvature is $R = 2(\mathcal{L} - F \mathcal{L}_F) = 2(\rho - p_\perp)$. We consider the general spherically symmetric metric ansatz

$$ds^2 = A(r) dt^2 - \frac{dr^2}{B(r)} - r^2 d\Omega^2, \quad (5)$$

such that

$$A(r) = \frac{1}{B(r)} = 1 - \frac{2\mathcal{M}(r)}{r}; \quad \mathcal{M}(r) = \frac{1}{2} \int_0^r \rho(x) x^2 dx, \quad (6)$$

where $d\Omega^2$ is the line element on a unit two-sphere. The solution we are interested in can be derived by choosing the density and pressure as

$$\rho(r) = \frac{q^2}{(r^2 + g^2)^2}; \quad p_\perp = \frac{q^2(r^2 - g^2)}{(r^2 + g^2)^3}; \quad g = \frac{\pi q^2}{8m}, \quad (7)$$

where g is the electromagnetic radius of the nonlinear electrodynamics (Dymnikova 2004). Then the Lagrangian and its derivative are

$$\mathcal{L} = \frac{2q^2(g^2 - r^2)}{(r^2 + g^2)^3}; \quad \mathcal{L}_F = \frac{(r^2 + g^2)^3}{r^6}. \quad (8)$$

Integration of Equation (3) with the density Equation (7) leads to the solution

$$A(r) = 1/B(r) = 1 - \frac{4m}{\pi r} \left[\arctan\left(\frac{r}{g}\right) - \frac{rg}{r^2 + g^2} \right], \quad (9)$$

where m is the mass of the black hole and g is a parameter that appears due to the coupling of nonlinear electrodynamics to general relativity (Dymnikova 2004). The metric Equation (9) is spherically symmetric and is also asymptotically flat as $\lim_{r \rightarrow \infty} A(r) = B(r) = 1$ and though regular everywhere for nonzero g , reduces to the singular Schwarzschild metric in the absence of nonlinear electrodynamics ($g = 0$). Asymptotically for $r \gg g$, metric Equation (9) reads as

$$A(r) = 1 - \frac{2m}{r} + \frac{q^2}{r^2} - \frac{2}{3} \frac{q^2 g^2}{r^4}, \quad (10)$$

and has a Reissner-Nordström limit as $r \rightarrow \infty$. At small values of r , $r \ll g$ we get de Sitter asymptotic with the cosmological constant $\Lambda = q^2/g^4$ which gives a useful expression for a cutoff on self-energy density by the finite value of the electromagnetic density T_0^0 ($r \rightarrow 0$) associated with the cosmological constant $\Lambda = 8\pi\rho(0)$, which emerges at the regular center. The mass of electromagnetic origin is related to this cutoff by $m = \pi^2 \rho(0) g^3$.

We approach the regularity problem of the solution by studying the behavior of invariant $R = R_a R^a$, Ricci scalar $\mathcal{R} = R_{ab} R^{ab}$, (R_{ab} Ricci tensor), and the Kretschmann scalar $K = R_{abcd} R^{abcd}$ (R_{abcd} Reimann tensor). They take the form

$$R = \frac{32mg^3}{\pi(r^2 + g^2)^3}, \quad \mathcal{R} = \frac{256m^2 g^2 (r^4 + g^4)}{\pi^2 (r^2 + g^2)^6}, \quad (11)$$

$$K = \frac{192m^2}{\pi^2 r^6 (r^2 + g^2)^6} (K_1 + K_2),$$

where

$$K_1 = (r^2 + g^2)^6 \left[\arctan\left(\frac{r}{g}\right) \right]^2 - 2 \left[\arctan\left(\frac{r}{g}\right) \right] rg (r^2 + g^2)^3 (3r^4 + \frac{8}{3}r^2 g^2 + g^4),$$

$$K_2 = r^2 g^2 \left(\frac{2}{3}r^4 + \frac{4}{3}r^2 g^2 + g^4 \right) (7r^4 + 4r^2 g^2 + g^4),$$

which are obviously well-behaved everywhere including as $r \rightarrow 0$, when $g, m \neq 0$ and $r \rightarrow 0$. At the center, they vanish. Thus, the spacetime Equation (5) is regular or nonsingular.

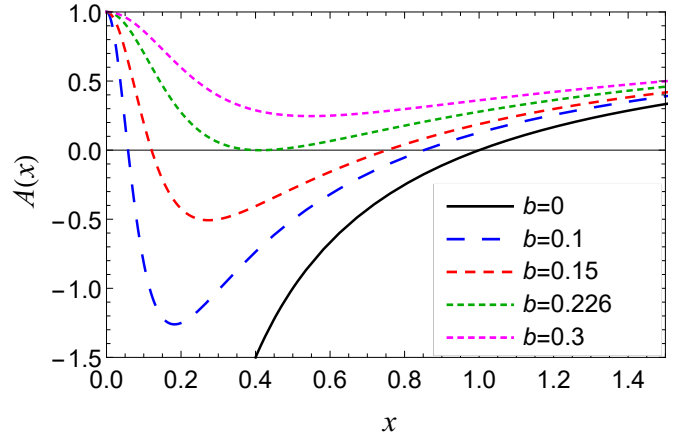


Figure 1. Plot showing $A(x)$ vs. x ; for $0 < b \leq b_E$ one has a black hole with two horizons while $b > b_E$ corresponds to no-horizon spacetime. Case $b = 0$ corresponds to the Schwarzschild black hole.

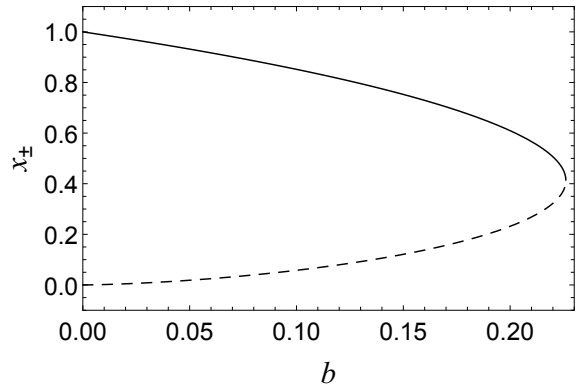


Figure 2. Locations of event horizon x_+ (solid line) and Cauchy horizon x_- (dashed line) for REC black holes.

2.1. Energy conditions and regularity

Next, we check the status of the various energy conditions using the prescription of Hawking & Ellis (2011) (Kothawala & Ghosh 2004; Ghosh & Kothawala 2008; Hawking & Ellis 2011). The Einstein equations governing the stress-energy tensor $T_{\mu\nu}$ are given by the Equation (3), which leads to

$$\rho = \frac{8mg}{\pi(r^2 + g^2)^2} = -P_r, \quad (12)$$

$$P_\theta = P_\phi = \frac{8mg(r^2 - g^2)}{\pi(r^2 + g^2)^3}. \quad (13)$$

The weak energy condition (WEC), $T_{\mu\nu}\xi^\mu\xi^\nu \geq 0$ for any timelike vector ξ^μ , which is equivalent to the findings in Hawking & Ellis (2011).

$$\rho \geq 0; \quad \rho + P_i \geq 0, \quad (i = r, \theta, \phi) \quad (14)$$

guarantees that the energy density as measured by any local observer is non-negative. Using the Eq. (9)

$$\rho + P_\theta = \rho + P_\phi = \frac{16mgr^2}{\pi(r^2 + g^2)^3}. \quad (15)$$

Hence, $\rho \geq 0$ and Eq.(15) imply that the WEC is satisfied everywhere.

Next, the dominant energy condition (DEC), $T^{00} \geq |T^{ki}|$ for each $i = r, \theta, \phi$, which holds if and only if (Hawking & Ellis 2011)

$$\rho \geq 0; \quad \rho + P_i \geq 0; \quad \rho - P_i \geq 0, \quad (i = r, \theta, \phi) \quad (16)$$

includes WEC and requires that each principal pressure $P_k = -T^i_i$ never exceeds the energy density. To check the DEC, we first calculate

$$\rho - P_\theta = \rho - P_\phi = \frac{16mg^3}{\pi(r^2 + g^2)^3}. \quad (17)$$

Thus, the DEC holds because of the WEC and Eq.(17). Lastly, the strong energy condition (SEC) requires (Hawking & Ellis 2011)

$$\rho + \sum_i P_i \geq 0 \quad (18)$$

and defines the sign of the gravitational acceleration. Thus, the SEC requires $\rho + P_r + 2 P_\theta \geq 0$. We find that

$$\rho + P_r + 2 P_\theta = \frac{16mg(r^2 - g^2)}{\pi(r^2 + g^2)^3} \quad (19)$$

which means that the SEC is satisfied when $r^2 > g^2$.

3. STRONG GRAVITATIONAL LENSING IN REC BLACK HOLE SPACETIME

We begin with rewriting the metric Equation (5) by redefining the quantities r, q and t in the units of radius $2m$ as

$$\begin{aligned} A(x) &= \frac{1}{B(x)} = 1 - \frac{2}{\pi x} \left[\arctan\left(\frac{x}{b}\right) - \frac{xb}{x^2 + b^2} \right], \\ C(x) &= x^2, \end{aligned} \quad (20)$$

where $b = g/2m$, $x = r/2m$ and $t = t/2m$. An elementary analysis of $A(x) = 0$ suggests a critical value of $b_E \approx 0.226$ corresponding to an extremal REC black hole (see Figure 1). On the other hand, $A(x) = 0$ has no positive root for $b > b_E$ and admits two distinct positive roots for $b < b_E$. They, respectively, describe no-horizon REC spacetime and non-extremal black holes. The critical point $b = b_E = 0.226$ corresponds to an extremal black hole with $A(x) = 0$ having equal

roots (see Figures 1 and 2). Further, in no-horizon REC spacetime, the photon sphere can exist when $b_E < b \leq b_P \approx 0.247$ and no photon sphere exists when $b > b_P$.

The strong field gravitational lensing is governed by the deflection angle and a lens equation. The null geodesic equation reads as

$$\left(\frac{dx}{d\tau}\right)^2 \equiv \dot{x}^2 = \mathcal{E}^2 - \frac{\mathcal{L}^2 A(x)}{C(x)}, \quad (21)$$

where the energy $\mathcal{E} = -p_\mu \xi_{(t)}^\mu$ and angular momentum $\mathcal{L} = p_\mu \xi_{(\phi)}^\mu$, with $\xi_{(t)}^\mu$ and $\xi_{(\phi)}^\mu$ are, respectively, the Killing vectors due to time-translational and rotational invariance. The radius of the photon sphere is the largest root found by Virbhadra & Ellis (2000) and Bozza (2002):

$$\frac{C'(x)}{C(x)} = \frac{A'(x)}{A(x)}, \quad (22)$$

which is depicted in the Figure 5. At the closest approach distance x_0 , $\dot{x}|_{x=x_0} = 0$ or $V_{\text{eff}}(x_0) = 0$, which leads to

$$u \equiv \frac{\mathcal{L}}{\mathcal{E}} = \sqrt{\frac{C(x_0)}{A(x_0)}}. \quad (23)$$

The effective potential from the radial Equation (21) reads as

$$\frac{V_{\text{eff}}}{\mathcal{E}^2} = \frac{u^2}{x^2} \left[1 - \frac{2}{\pi x} \left(\arctan\left(\frac{x}{b}\right) - \frac{xb}{x^2 + b^2} \right) \right] - 1. \quad (24)$$

It turns out that a light ray exists in the region where $V_{\text{eff}} \leq 0$ (see Figures 3 and 4). Further, one can define an unstable (or a stable circular orbit) satisfying $V_{\text{eff}} = V'_{\text{eff}}(x) = 0$ and $V''_{\text{eff}}(x_{\text{ps}}) < 0$ (or $V''_{\text{eff}}(x_{\text{ps}}) > 0$). For REC spacetime, we find that $V''_{\text{eff}}(x_{\text{ps}}) < 0$, which corresponds to the unstable photon circular orbits (see Figures 3 and 4).

The deflection angle becomes unboundedly large at $x_0 = x_{\text{ps}}$ and is finite only for $x_0 > x_{\text{ps}}$. The critical impact parameter u_{ps} is defined as (Bozza 2002)

$$u_{\text{ps}} = \sqrt{\frac{C(x_{\text{ps}})}{A(x_{\text{ps}})}}, \quad (25)$$

and depicted in Figure 5. This is the impact parameter for which the photon approaches the black hole with the closest approach distance $x_0 = x_{\text{ps}}$ and revolves around it in an unstable circular orbit of radius x_{ps} . The photons that have impact parameter $u < u_{\text{ps}}$ fall into the black hole, while photons with impact parameter $u > u_{\text{ps}}$ reach the minimum distance x_0 near the black hole and then are symmetrically scattered to infinity.

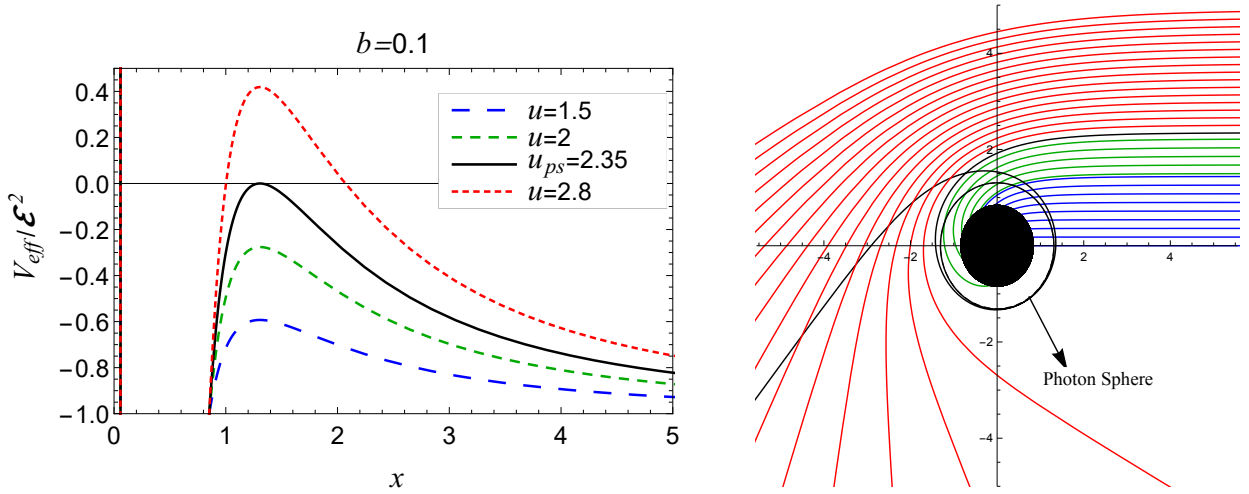


Figure 3. (a) (left) Variation of the effective potential V_{eff} for REC black holes as a function of radial coordinate x . The photons with critical impact parameter (u_{ps}) (black solid curve) make unstable circular orbits. (b) (right) Trajectories of photons for REC black holes with different impact parameters u . Photons having impact parameter $u > u_{\text{ps}}$ (red curves) are scattered to infinity, while photons impacted by parameter $u < u_{\text{ps}}$ (green and blue curves) are absorbed in the black hole. Photons with an impact parameter almost close to the critical impact parameter $u \approx u_{\text{ps}}$ (black curve) make several loops around the black hole before being scattered to infinity.

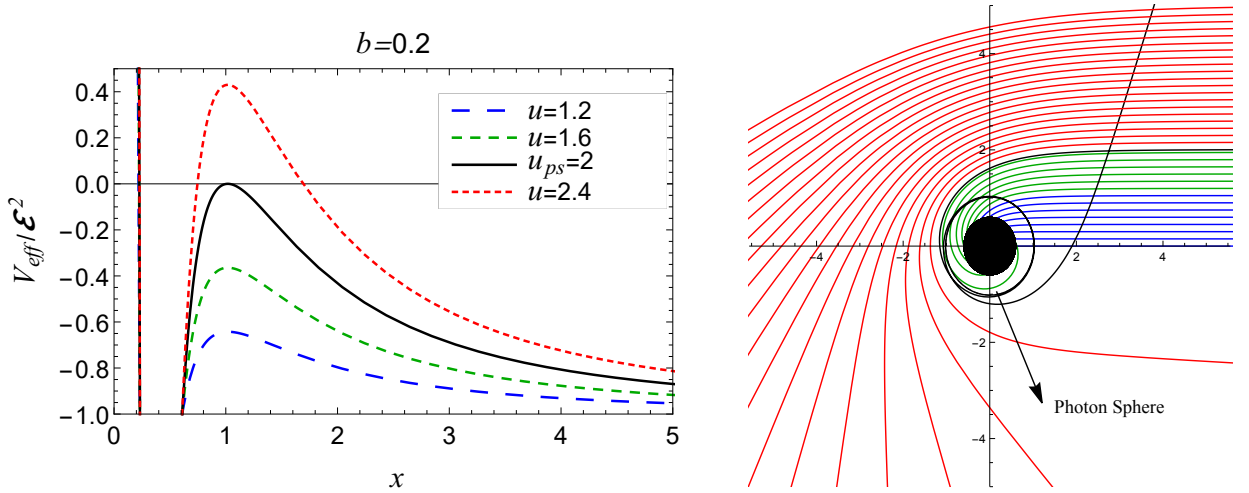


Figure 4. (a) (left) Variation of the effective potential V_{eff} for REC black holes as a function of radial coordinate x . The photons with critical impact parameter (u_{ps}) (black solid curve) make unstable circular orbits. (b) (right) Trajectories of photons for REC black holes having different impact parameters u . A Photon with impact parameter $u > u_{\text{ps}}$ (red curves) is scattered to infinity, while the photon impacted by parameter $u < u_{\text{ps}}$ (green and blue curves) is absorbed in the black hole. A photon with an impact parameter almost close to the critical impact parameter $u \approx u_{\text{ps}}$ (black curve) makes several loops around the black hole before being scattered to infinity.

The deflection angle, as a function of the closest approach distance x_0 , for the spacetime Equation (5) reads as (Virbhadrá & Ellis 2002)

$$\alpha_D(x_0) = I(x_0) - \pi = 2 \int_{x_0}^{\infty} \frac{\sqrt{B(x)} dx}{\sqrt{C(x)} \sqrt{\frac{C(x)A(x_0)}{C(x_0)A(x)} - 1}} - \pi. \quad (26)$$

Next, let us define a new variable $z = 1 - x_0/x$ (Bozza 2002; Chen & Jing 2009; Kumar et al. 2022b) and using

the relation between the impact parameter u and closest approach distance x_0 , the deflection angle as a function of the impact parameter u in strong field limit yields

$$\alpha_D(u) = -\bar{a} \log \left(\frac{u}{u_{\text{ps}}} - 1 \right) + \bar{b} + \mathcal{O}(u - u_{\text{ps}}) \log(u - u_{\text{ps}}), \quad (27)$$

where $u \approx \theta D_{\text{OL}}$. \bar{a} and \bar{b} are the lensing coefficients as depicted in Figure 6, the calculations for which are

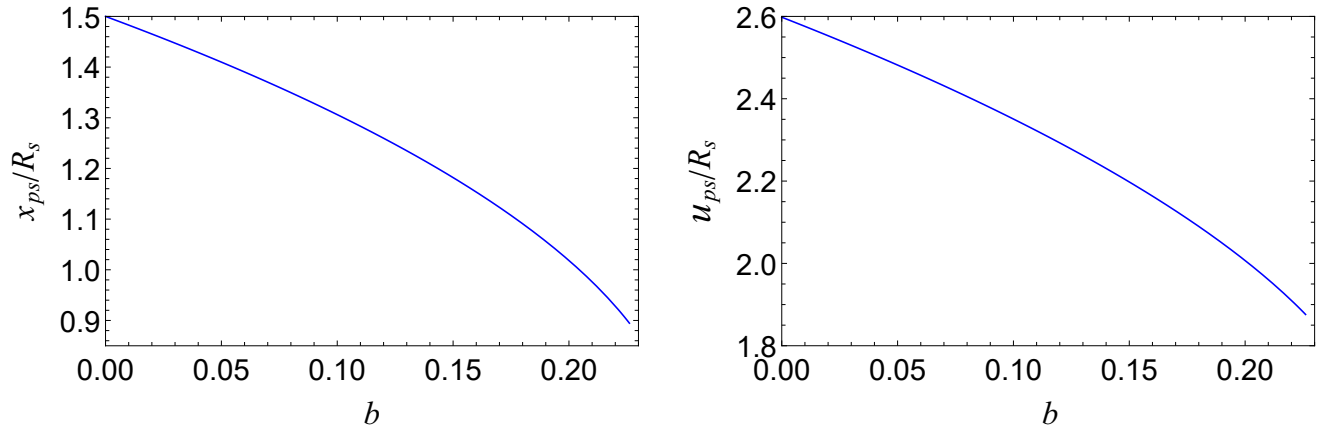


Figure 5. Behavior of the photon sphere radius x_{ps} (left) and the critical impact parameter u_{ps} (right) for REC black hole spacetime as a function of the parameter b . As $b \rightarrow 0$, the values $x_{\text{ps}} \rightarrow 1.5$ and $u_{\text{ps}} \rightarrow 2.598$ correspond to a Schwarzschild black hole (Bozza 2002).

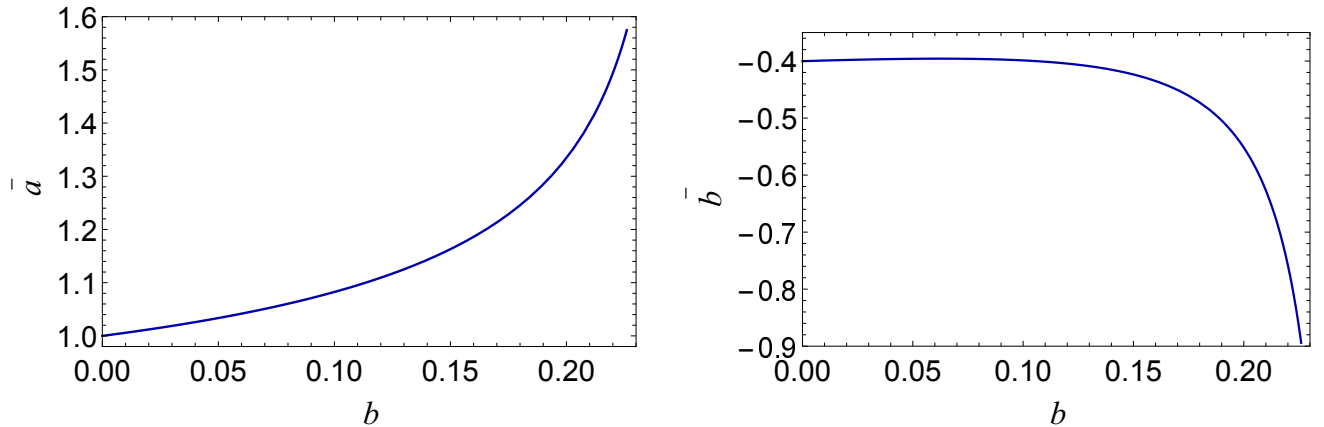


Figure 6. Behavior of strong lensing coefficients \bar{a} and \bar{b} for REC black hole spacetime as a function of the parameter b . $\bar{a} = 1$ and $\bar{b} = -0.4002$ at $b = 0$ correspond to the values of a Schwarzschild black hole.

given in (Bozza 2002). The deflection angle $\alpha_D(u)$ as a function of u for different b is depicted in Figure 7.

The deflection angle for REC black holes (Equation (5)) (see Figure 7) is monotonically decreasing with impact parameter u and deflection angle $\alpha_D(u) \rightarrow \infty$ as $u \rightarrow u_{\text{ps}}$. Interestingly, the deflection angle for REC black holes decreases with the increasing value of the parameter b whereas for an impact parameter close to the critical impact parameter (see Figure 7), the deflection angle $\alpha_D(b)$ increases with b . The two infinite sets of relativistic images correspond, respectively, to clockwise and counterclockwise winding around the black hole. When $x_0 \approx x_{\text{ps}}$, the leading term of the divergence is z^{-1} (Bozza 2002); thus, the integral diverges logarithmically. The coefficient \bar{a} increases while \bar{b} decreases with the increasing value of b (see Figure 6) and $\bar{a} = 1$ and $\bar{b} = -0.4002$ (Bozza 2002; Islam et al. 2020) correspond to the case of a Schwarzschild black hole (see Table 1).

Lensing Coefficients			
b	\bar{a}	\bar{b}	u_{ps}/R_s
0	1.0000	-0.40023	2.59808
0.05	1.03352	-0.39609	2.48181
0.1	1.08253	-0.39889	2.35072
0.15	1.16297	-0.423537	2.19784
0.2	1.33445	-0.551714	2.00694
0.22	1.49388	-0.758393	1.90995

Table 1. Estimates for the strong Lensing Coefficients \bar{a} , \bar{b} and the critical impact parameter u_{ps}/R_s for REC Black Hole Spacetime. The values for $b = 0$ correspond to a Schwarzschild black hole.

We assume that the source and observer are far from the black hole (lens) and they are perfectly aligned. The asymptotically flat lens equation reads as (Bozza et al.

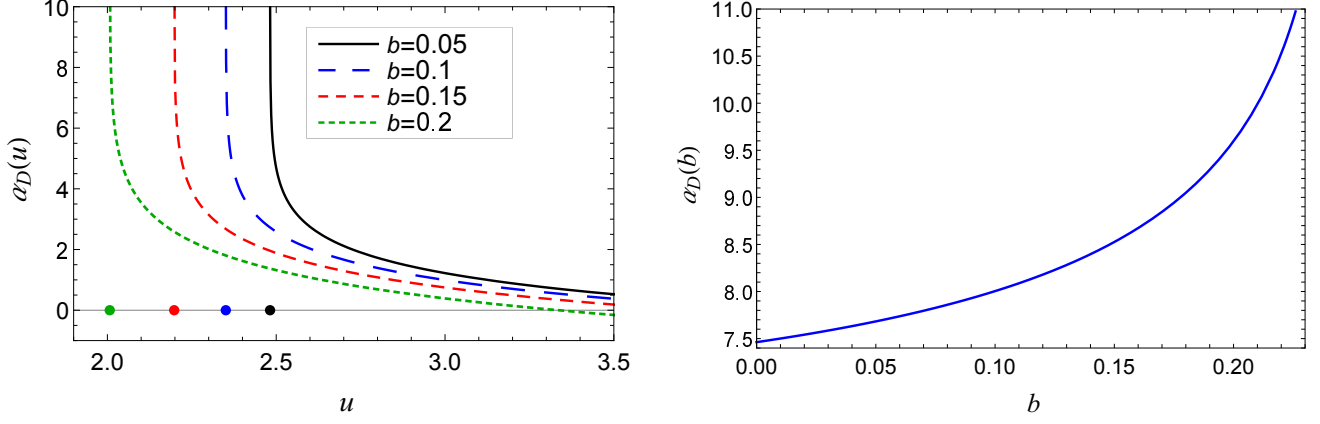


Figure 7. (a) (left) Variation of deflection angle for REC black hole spacetime as a function of the impact parameter u for different values of parameter b . Dots on the horizontal axis represent the values of the impact parameter $u = u_{\text{ps}}$ at which the deflection angle diverges. (b) (right) Deflection angles for REC black hole spacetime evaluated at $u = u_{\text{ps}} + 0.001$ as a function of parameter b .

2001)

$$\beta = \theta - \frac{D_{LS}}{D_{OS}} \Delta\alpha_n, \quad (28)$$

where $\Delta\alpha_n = \alpha - 2n\pi$ is the offset of deflection angle looping over $2n\pi$ and n is an integer. Here, β is the angular position of the source while θ is the angular position of the image from the optic axis. The distance between the observer and the lens and between the observer and the source are D_{OL} and D_{OS} , respectively. Using Equations (27) and (28), the position of the n th relativistic image can be approximated as (Bozza 2002)

$$\theta_n = \theta_n^0 + \frac{u_{\text{ps}} e_n (\beta - \theta_n^0) D_{OS}}{\bar{a} D_{LS} D_{OL}}, \quad (29)$$

where

$$e_n = \exp\left(\frac{\bar{b}}{\bar{a}} - \frac{2n\pi}{\bar{a}}\right), \quad (30)$$

θ_n^0 are the image positions corresponding to $\alpha = 2n\pi$.

As gravitational lensing conserves surface brightness, the magnification is the quotient of the solid angles subtended by the n th image, and the source (Virbhadrha & Ellis 2000; Bozza 2002; Virbhadrha 2009). The magnification of the n th relativistic image reads as (Bozza 2002)

$$\mu_n = \left(\frac{\beta}{\theta} \frac{d\beta}{d\theta}\right)^{-1} \Bigg|_{\theta_n^0} = \frac{u_{\text{ps}}^2 e_n (1 + e_n) D_{OS}}{\bar{a} \beta D_{LS} D_{OL}^2}. \quad (31)$$

The first relativistic image is the brightest one, and the magnifications decrease exponentially with n . The magnifications are proportional to $1/D_{OL}^2$, which is a very small factor and thus the relativistic images are very faint, unless β has values close to zero, i.e. nearly perfect alignment.

Having obtained the deflection angle (Equation (27)) and lens equation (Equation (28)), we calculate three observables of relativistic images (see Table 2, Figures 8 and 10), the angular position of the asymptotic relativistic images (θ_∞), the angular separation between the outermost and asymptotic relativistic images (s) (see Figure 8) and relative magnification of the outermost relativistic image with other relativistic images (r_{mag}) (Bozza 2002; Islam et al. 2021)

$$\theta_\infty = \frac{u_{\text{ps}}}{D_{OL}}, \quad (32)$$

$$s = \theta_1 - \theta_\infty = \theta_\infty \exp\left(\frac{\bar{b}}{\bar{a}} - \frac{2\pi}{\bar{a}}\right), \quad (33)$$

$$r_{\text{mag}} = \frac{5\pi}{\bar{a} \log(10)}. \quad (34)$$

The strong deflection limit coefficients \bar{a} , \bar{b} and the critical impact parameter u_{ps} can be obtained after measuring s , r_{mag} and θ_∞ . If θ_∞ represents the asymptotic position of a set of images in the limit $n \rightarrow \infty$, we consider that only the outermost image θ_1 is resolved as a single image and all the remaining ones are packed together at θ_∞ . The values obtained from measurements can be compared with those predicted by the theoretical models to check the nature of the black hole.

3.1. Einstein ring

When a source in front of the lens can generate relativistic images and Einstein rings (Luminet 1979), and the gravitational field leads to an Einstein ring if the source, lens, and observer are flawlessly aligned. However, it is adequate that just one source point is flawlessly aligned to build a complete relativistic

Table 2. Estimates for the Lensing Observables of Primary Images for REC Black Hole Spacetime as Compared with Schwarzschild Spacetime ($b = 0$) Considering the Supermassive Black Holes Sgr A*, M87*, NGC 4649, and NGC 1332 as a Lens. The observable r_{mag} does not depend upon the mass or distance of the black hole from the observer.

b	Sgr A*		M87*		NGC 4649		NGC 1332		r_{mag}
	$\theta_\infty(\mu\text{as})$	$s(\mu\text{as})$	$\theta_\infty(\mu\text{as})$	$s(\mu\text{as})$	$\theta_\infty(\mu\text{as})$	$s(\mu\text{as})$	$\theta_\infty(\mu\text{as})$	$s(\mu\text{as})$	
0.0	26.3299	0.0329517	19.782	0.0247571	14.6615	0.0183488	7.76719	0.00972061	6.82188
0.05	25.1516	0.039254	18.8968	0.0294921	14.0054	0.0218582	7.41962	0.0115797	6.60061
0.1	23.8231	0.0496879	17.8987	0.0373313	13.2657	0.0276682	7.02771	0.0146577	6.3018
0.15	22.2737	0.0697065	16.7346	0.0523715	12.4029	0.0388154	6.57066	0.0205631	5.86589
0.2	20.339	0.121317	15.281	0.0911474	11.3256	0.0675542	5.99993	0.035788	5.11214
0.22	19.3561	0.173666	14.5425	0.130478	10.7783	0.0967039	5.70997	0.0512306	4.56657

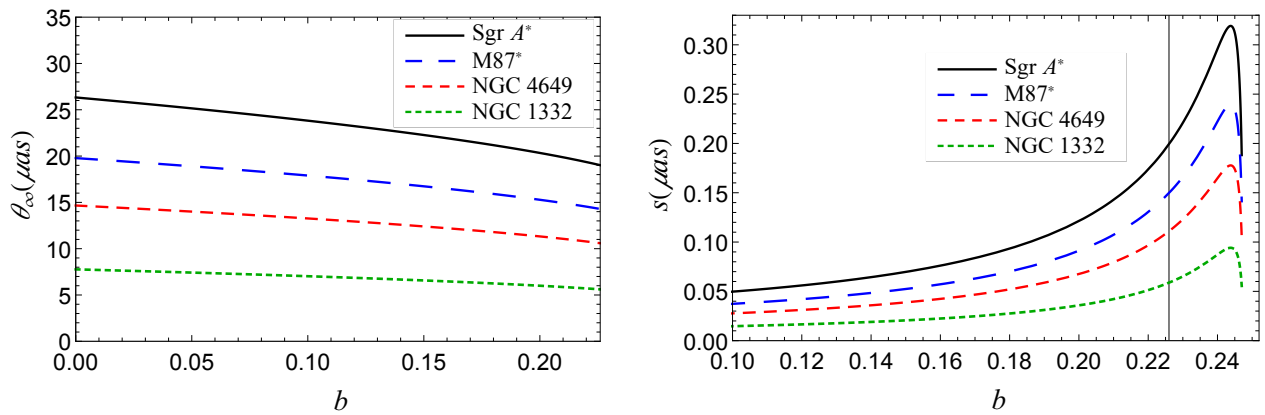


Figure 8. Behavior of lensing observables θ_∞ (left), s (right) as a function of the parameter b in strong field limit by considering that the spacetime around the compact objects at the centers of nearby galaxies is REC spacetime. The vertical black line corresponds to the extremal black hole for $b = b_E \approx 0.226$. For no-horizon spacetime ($b > b_E$), separation s increases with b to reach a maximum and then decreases. On the other hand, for REC black holes ($0 < b < b_E$), it has an increasing behavior.

Einstein ring (Bozza & Mancini 2004a). Thus, if the source, lens, and observer are aligned (such that $\beta = 0$), then the Equation (29) accepts the form

$$\theta_n^E = \left(1 - \frac{D_{OS}}{D_{LS}} \frac{u_{ps} e_n}{D_{OL} \tilde{a}}\right) \theta_n^0, \quad (35)$$

which solves to give the radii of the Einstein rings. Equation (35) for a special case when the lens is equidistant between the source and observer, yields

$$\theta_n^E = \left(1 - \frac{2u_{ps} e_n}{D_{OL} \tilde{a}}\right) \left(\frac{u_{ps}}{D_{OL}} (1 + e_n)\right). \quad (36)$$

Since $D_{OL} \gg u_m$, the Eq. (36) yields

$$\theta_n^E = \frac{u_{ps}}{D_{OL}} (1 + e_n), \quad (37)$$

which gives the radius of the n th relativistic Einstein ring. Note that $n = 1$ portrays the outermost ring, and as n increases, the radius of the ring decreases. Also, it can be conveniently specified from Eq. (37) that the

Einstein ring's radius increases with the black hole's mass and declines as the distance between the observer and lens increases. In Figure 9, we plot the outermost relativistic Einstein rings of Sgr A*, M87* NGC 4649, and NGC 1332.

4. TIME DELAY IN STRONG FIELD LIMIT

The time difference is caused by the photon taking different paths while winding the black hole, so there is a time delay between different images. If we can distinguish the time signals of the first image and other packed images, we can calculate their time delay (Bozza & Mancini 2004b). The time spent by the photon to wind around the black hole is (Bozza & Mancini 2004b)

$$\tilde{T}(u) = \tilde{a} \log\left(\frac{u}{u_{ps}} - 1\right) + \tilde{b} + \mathcal{O}(u - u_{ps}). \quad (38)$$

The images are highly demagnified, and the separation between the images is of the order of microarcseconds, so we must at least distinguish the

Table 3. Estimation of time delay for supermassive black holes at the center of nearby galaxies considering them as representing Schwarzschild and REC black hole spacetime ($b = 0.2$). Mass (M) and distance (D_{OL}) are given in units of solar mass and megaparsec, respectively. Time Delays are expressed in minutes.

Galaxy	$M(M_{\odot})$	D_{OL} (Mpc)	M/D_{OL}	$\Delta T_{2,1}^s$ (Schw.)	$\Delta T_{2,1}^s$ (REC)
Milky Way	4.3×10^6	0.0083	2.471×10^{-11}	11.4968	8.88091
M87	6.5×10^9	16.68	1.758×10^{-11}	17378.8	12701.8
NGC 4472	2.54×10^9	16.72	7.246×10^{-12}	6791.11	5245.94
NGC 1332	1.47×10^9	22.66	3.094×10^{-12}	3930.29	3036.03
NGC 4374	9.25×10^8	18.51	2.383×10^{-12}	2473.14	1910.43
NGC 1399	8.81×10^8	20.85	2.015×10^{-12}	2355.5	1819.55
NGC 3379	4.16×10^8	10.70	1.854×10^{-12}	1112.25	859.177
NGC 4486B	6×10^8	16.26	1.760×10^{-12}	1604.2	1239.2
NGC 1374	5.90×10^8	19.57	1.438×10^{-12}	1577.46	1218.54
NGC 4649	4.72×10^9	16.46	1.367×10^{-12}	12619.7	9748.35
NGC 3608	4.65×10^8	22.75	9.750×10^{-13}	1243.26	960.378
NGC 3377	1.78×10^8	10.99	7.726×10^{-13}	475.913	367.629
NGC 4697	2.02×10^8	12.54	7.684×10^{-13}	540.081	417.196
NGC 5128	5.69×10^7	3.62	7.498×10^{-13}	152.132	117.517
NGC 1316	1.69×10^8	20.95	3.848×10^{-13}	451.85	349.041
NGC 3607	1.37×10^8	22.65	2.885×10^{-13}	366.292	282.95
NGC 4473	0.90×10^8	15.25	2.815×10^{-13}	240.63	185.88
NGC 4459	6.96×10^7	16.01	2.073×10^{-13}	186.087	143.747
M32	2.45×10^6	0.8057	1.450×10^{-13}	6.55048	5.06006
NGC 4486A	1.44×10^7	18.36	3.741×10^{-14}	38.5008	29.7407
NGC 4382	1.30×10^7	17.88	3.468×10^{-14}	34.7577	26.8493
CYGNUS A	2.66×10^9	242.7	1.4174×10^{-15}	7111.95	5493.78

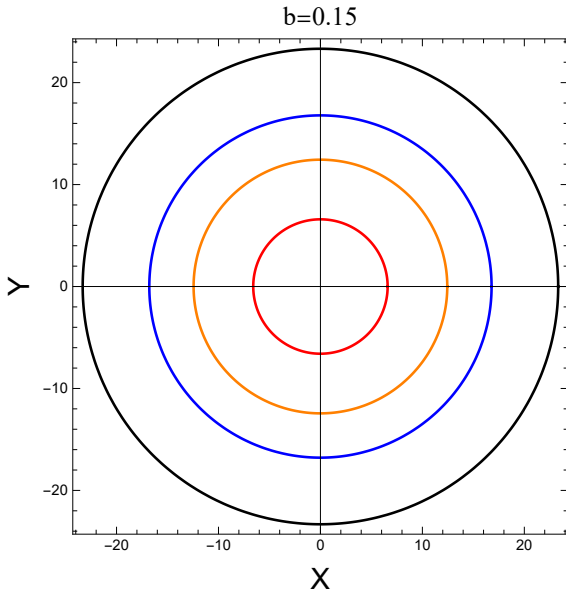


Figure 9. Einstein rings for different compact objects at the centers of nearby galaxies by considering them to be REC black holes. Black, blue, orange and red rings correspond to Sgr A*, M87*, NGC 4649 and NGC 1332.

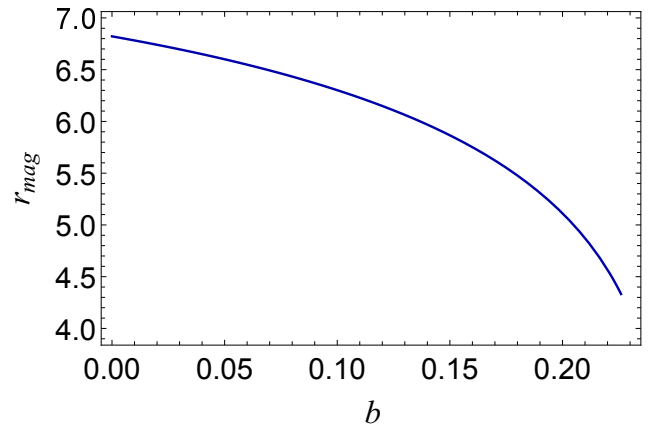


Figure 10. Behavior of strong lensing observable r_{mag} , for REC black hole spacetime as a function of the parameter b . It is independent of the black hole's mass or distance from the observer.

outermost relativistic image from the rest, and we assume the source to be variable, which generally are abundant in all galaxies, otherwise, there is no time delay to measure. For spherically symmetric black holes, the time delay between the first and second

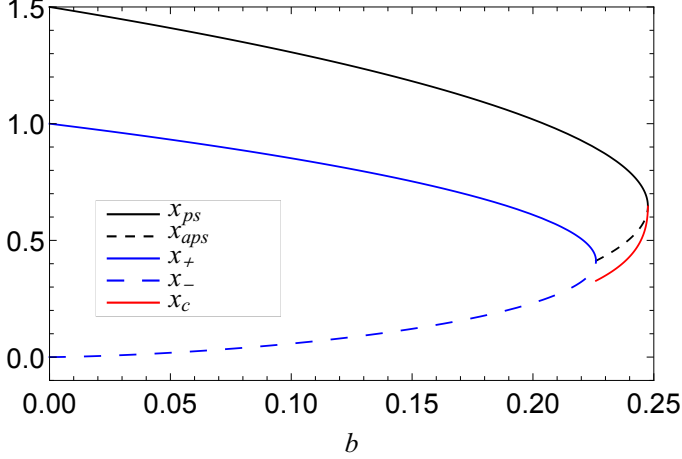


Figure 11. Locations of photon sphere x_{ps} (black solid line), anti-photon sphere x_{aps} (black dashed line), event horizon x_+ (blue solid line), Cauchy horizon x_- (blue dashed line) and smaller positive root of V_{eff} for $u = u_{\text{ps}}$ (red solid curve) for REC no-horizon spacetime.

relativistic image reads as

$$\Delta T_{2,1}^s = 2\pi u_{\text{ps}} = 2\pi D_{\text{OL}} \theta_{\infty}. \quad (39)$$

Using Eq. (39), if we can measure the time delay with an accuracy of 5% and the critical impact parameter with negligible error, we can obtain the distance of the black hole with an accuracy of 5%. In Table 3, we compare $\Delta T_{2,1}^s$ for the supermassive black holes at the center of several galaxies representing Schwarzschild and REC black hole spacetime.

5. STRONG GRAVITATIONAL LENSING IN REC NO-HORIZON SPACETIMES

Next, we investigate gravitational lensing in the strong deflection limit by REC no-horizon spacetime with $b_E < b \leq b_P$. Since there is no horizon, photons with impact parameter $u < u_{\text{ps}}$ need not necessarily fall to the center and as there exists a potential barrier near x_c (see Figures 11 and 12), where x_c is the smaller positive root of V_{eff} for $u = u_{\text{ps}}$, the photons will emerge after reaching the closest approach distance $x_0 \approx x_c$. Thereby, the lensing will occur not only from the outside but also from the inside of the photon sphere (see Figure 12), resulting in two sets of infinite images, created by lensing from the outside and the inside of the photon sphere. The lensing from outside of photon sphere is exactly similar to the black hole case and the prescription given in Section 3 remains valid.

5.1. Lensing from inside the photon sphere

In this case, the impact parameter u of the photon is less than the critical value u_{ps} . Due to the presence of

the potential barrier near x_c , the photon, after entering inside the photon sphere, gets reflected at the closest approach distance $x_0 \approx x_c$ and exits toward the ∞ .

The deflection angle as a function of the impact parameter u is given by Shaikh et al. (2019) as

$$\alpha_D(u) = -\bar{p} \log \left(\frac{u_{\text{ps}}^2}{u^2} - 1 \right) + \bar{q} + \mathcal{O}((u_{\text{ps}}^2 - u^2) \log(u_{\text{ps}}^2 - u^2)), \quad (40)$$

where

$$\bar{p} = 2 \sqrt{\frac{2B(x_{\text{ps}})A(x_{\text{ps}})}{C''(x_{\text{ps}})A(x_{\text{ps}}) - C(x_{\text{ps}})A''(x_{\text{ps}})}}, \quad (41)$$

$$\bar{q} = \bar{p} \log \left[2x_{\text{ps}}^2 \left(\frac{C''(x_{\text{ps}})}{C(x_{\text{ps}})} - \frac{A''(x_{\text{ps}})}{A(x_{\text{ps}})} \right) \left(\frac{x_{\text{ps}}}{x_c} - 1 \right) \right] + I_R(x_c) - \pi. \quad (42)$$

Figure 13 shows the deflection angle for no-horizon spacetime. Unlike in the case of a black hole, photons with the impact parameter $u < u_{\text{ps}}$ are also lensed. A photon lensed from the inside of the photon sphere is represented by the curves on the left of the dots, while photon lensing from the outside of the photon sphere is depicted by the curves on the right of the dots. Using Eq's. (28) and (40), the angular position of the n th relativistic image formed from the inside of the photon sphere can be written as (Shaikh et al. 2019)

$$\theta_{-n} = \theta_{-n}^0 - \frac{u_{\text{ps}} e_{-n} (\beta - \theta_{-n}^0) D_{\text{OS}}}{2\bar{p} D_{\text{LS}} D_{\text{OL}} (1 + e_{-n})^{\frac{3}{2}}}, \quad (43)$$

where

$$\theta_{-n}^0 = \frac{u_{\text{ps}}}{D_{\text{OL}}} \frac{1}{\sqrt{1 + e_{-n}}}, \quad (44)$$

and

$$e_{-n} = \exp \left(\frac{\bar{q} - 2n\pi}{\bar{p}} \right). \quad (45)$$

The correction to θ_{-n}^0 is negligible compared to θ_{-n}^0 . Therefore, the angular positions of the images are approximated by θ_{-n}^0 in order to calculate the observables such as separation and magnifications of the images.

We define separation s_{-n} as

$$s_{-n} = \theta_{\infty} - \theta_{-n}, \quad (46)$$

which is the angular separation between the n th image formed by lensing from the inside of the photon sphere and the image corresponding to the impact parameter $u = u_{\text{ps}}$. s_1 is defined as the angular separation between the first image formed by lensing from the

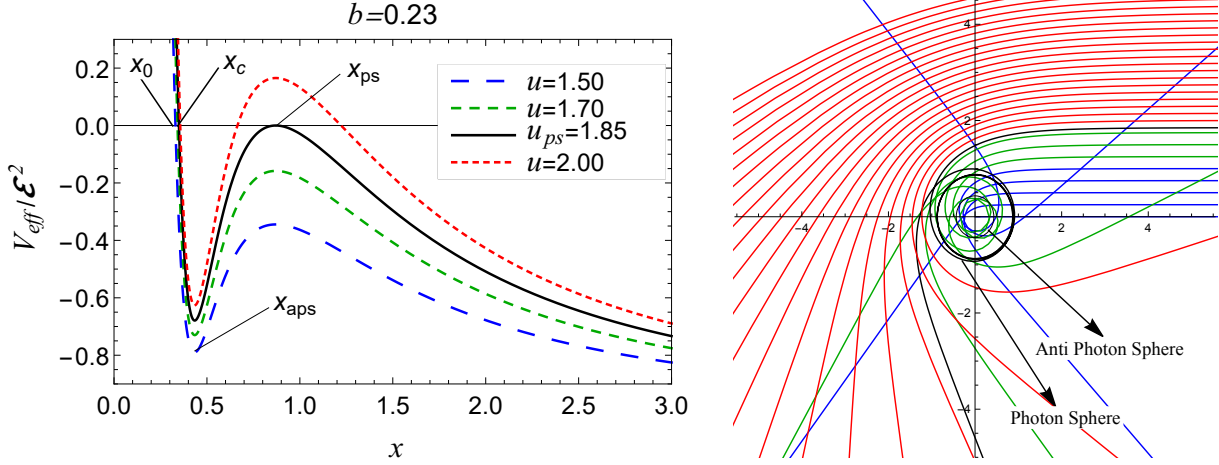


Figure 12. (a) (left) V_{eff} for REC no-horizon spacetime ($b = 0.23$). x_{ps} and x_{aps} are the locations of the photon sphere and anti-photon sphere respectively. For a photon, that has the impact parameter $u < u_{\text{ps}}$, the closest approach distance x_0 is close to x_c , where x_c is the smaller positive root of V_{eff} for $u = u_{\text{ps}}$. (b) (right) Trajectories of photons for REC no-horizon spacetime with different impact parameters u . Photons with impact parameter $u > u_{\text{ps}}$ (red curves) are scattered to infinity after reaching the closest approach distance x_0 , which is greater than x_{ps} . At the same time, the photons having impact parameter $u < u_{\text{ps}}$ (green and blue curves) enter inside the photon sphere and are scattered to infinity after reaching the closest approach distance x_0 , which is close to x_c . A photon with an impact parameter almost close to the critical impact parameter $u \approx u_{\text{ps}}$ (black curve) makes several loops around the centre before being scattered to infinity. The inner black circular curve shows the location of the anti-photon sphere.

Table 4. Magnifications of first-order and second-order relativistic images due to lensing by Sgr A* with $d = D_{\text{LS}}/D_{\text{OS}} = 0.5$: Schwarzschild and REC black hole spacetime ($b = 0.2$) predictions for magnifications μ_n are given for different values of angular source position β . (a) 1p and 1s refer to first-order relativistic images on the same side as primary and secondary images, respectively. (b) We have used $M_{\text{Sgr A}^*} = 4.3 \times 10^6$ m, $D_{\text{OL}} = 8.35 \times 10^3$ pc (c) Angular positions of first-order relativistic images for Schwarzschild and REC black hole spacetime are, respectively, $\theta_{1p,\text{SCH}} \approx -\theta_{1s,\text{SCH}} \approx 26.3299\mu\text{as}$ and $\theta_{1p,\text{DM}} \approx -\theta_{1s,\text{DM}} \approx 20.339\mu\text{as}$ and are highly insensitive to the angular source position β .

$\beta(\mu\text{as})$	REC black hole spacetime				Schwarzschild spacetime			
	$\mu_{1p,\text{DM}}$	$\mu_{2p,\text{DM}}$	$\mu_{1s,\text{DM}}$	$\mu_{2s,\text{DM}}$	$\mu_{1p,\text{SCH}}$	$\mu_{2p,\text{SCH}}$	$\mu_{1s,\text{SCH}}$	$\mu_{2s,\text{SCH}}$
10^0	1.80359×10^{-11}	1.61705×10^{-13}	-1.80359×10^{-11}	-1.61705×10^{-13}	8.52495×10^{-12}	1.59×10^{-14}	-8.52495×10^{-12}	-1.59×10^{-14}
10^1	1.80359×10^{-12}	1.61705×10^{-14}	-1.80359×10^{-12}	-1.61705×10^{-14}	8.52495×10^{-13}	1.59×10^{-15}	-8.52495×10^{-13}	-1.59×10^{-15}
10^2	1.80359×10^{-13}	1.61705×10^{-15}	-1.80359×10^{-13}	-1.61705×10^{-15}	8.52495×10^{-14}	1.59×10^{-16}	-8.52495×10^{-14}	-1.59×10^{-16}
10^3	1.80359×10^{-14}	1.61705×10^{-16}	-1.80359×10^{-14}	-1.61705×10^{-16}	8.52495×10^{-15}	1.59×10^{-17}	-8.52495×10^{-15}	-1.59×10^{-17}
10^4	1.80359×10^{-15}	1.61705×10^{-17}	-1.80359×10^{-15}	-1.61705×10^{-17}	8.52495×10^{-16}	1.59×10^{-18}	-8.52495×10^{-16}	-1.59×10^{-18}

outside of the photon sphere and the image corresponding to the impact parameter $u = u_{\text{ps}}$. We find that the first three images formed by lensing from the inside of the photon sphere are well separated in comparison to the images formed by lensing from the outside of the photon sphere. We define relative magnification \mathcal{R}_1 for the first image formed from the outside of the photon sphere as (Shaikh et al. 2019)

$$\mathcal{R}_1 = 2.5 \log \frac{\mu_1}{\sum_{m=2}^{\infty} \mu_m + \sum_{m=4}^{\infty} |\mu_{-m}|} \quad (47)$$

and relative magnification \mathcal{R}_{-n} for the first three images formed from the inside of the photon sphere as

(Shaikh et al. 2019)

$$\mathcal{R}_{-n} = 2.5 \log \frac{|\mu_{-n}|}{\sum_{m=2}^{\infty} \mu_m + \sum_{m=4}^{\infty} |\mu_{-m}|} \quad (n = 1, 2, 3) \quad (48)$$

where

$$\sum_{m=2}^{\infty} \mu_m = \frac{u_{\text{ps}}^2 D_{\text{OS}}}{\bar{a} \beta D_{\text{OL}}^2 D_{\text{LS}}} \frac{\exp\left(\frac{\bar{b}}{a}\right) \left[\exp\left(\frac{4\pi}{a}\right) + \exp\left(\frac{2\pi}{a}\right) + \exp\left(\frac{\bar{b}}{a}\right) \right]}{\exp\left(\frac{4\pi}{a}\right) \left[\exp\left(\frac{4\pi}{a}\right) - 1 \right]} \quad (49)$$

Table 5. Magnifications of first- and second-order relativistic images due to lensing by M87* with $d = D_{LS}/D_{OS} = 0.5$: Schwarzschild and REC black hole spacetime ($b = 0.2$) predictions for magnifications μ_n are given for different values of angular source position β . (a) $1p$ and $1s$ refer to first-order relativistic images on the same side as primary and secondary images, respectively. (b) We have used $M_{M87^*} = 6.5 \times 10^9$ m, $D_{OL} = 16.8 \times 10^6$ pc. (c) Angular positions of first-order relativistic images for Schwarzschild and REC black hole spacetime are, respectively, $\theta_{1p,SCH} \approx -\theta_{1s,SCH} \approx 19.8068 \mu\text{as}$ and $\theta_{1p,DM} \approx -\theta_{1s,DM} \approx 15.3722 \mu\text{as}$ and are highly insensitive to the angular source position β .

$\beta(\mu\text{as})$	REC black hole spacetime				Schwarzschild spacetime			
	$\mu_{1p,DM}$	$\mu_{2p,DM}$	$\mu_{1s,DM}$	$\mu_{2s,DM}$	$\mu_{1p,SCH}$	$\mu_{2p,SCH}$	$\mu_{1s,SCH}$	$\mu_{2s,SCH}$
10^0	1.01808×10^{-11}	9.12786×10^{-14}	-1.01808×10^{-11}	-9.12786×10^{-14}	4.75466×10^{-12}	8.86797×10^{-15}	-4.75466×10^{-12}	-8.86797×10^{-15}
10^1	1.01808×10^{-12}	9.12786×10^{-15}	-1.01808×10^{-12}	-9.12786×10^{-15}	4.75466×10^{-13}	8.86797×10^{-16}	-4.75466×10^{-13}	-8.86797×10^{-16}
10^2	1.01808×10^{-13}	9.12786×10^{-16}	-1.01808×10^{-13}	-9.12786×10^{-16}	4.75466×10^{-14}	8.86797×10^{-17}	-4.75466×10^{-14}	-8.86797×10^{-17}
10^3	1.01808×10^{-14}	9.12786×10^{-17}	-1.01808×10^{-14}	-9.12786×10^{-17}	4.75466×10^{-15}	8.86797×10^{-18}	-4.75466×10^{-15}	-8.86797×10^{-18}
10^4	1.01808×10^{-15}	9.12786×10^{-18}	-1.01808×10^{-15}	-9.12786×10^{-18}	4.75466×10^{-16}	8.86797×10^{-19}	-4.75466×10^{-16}	-8.86797×10^{-19}

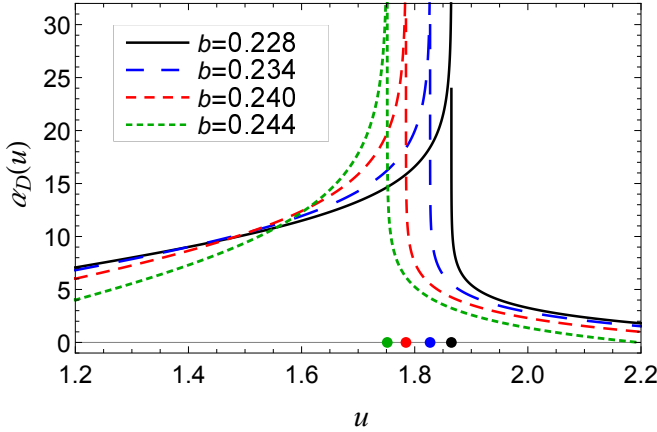


Figure 13. Deflection angle for REC no-horizon spacetime as a function of the impact parameter u . Dots on the horizontal axis represent the values of the critical impact parameter u_{ps} at which the deflection angle diverges. The curves on the left of the dots represent strong lensing from the inside of the photon sphere ($u < u_{ps}$), while the curves on the right represent strong lensing from the outside of the photon sphere ($u > u_{ps}$).

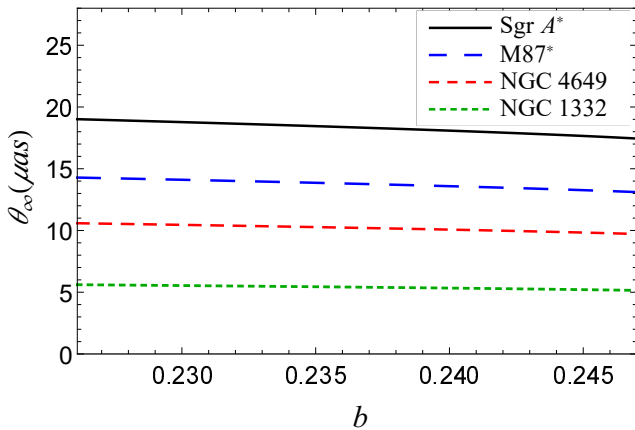


Figure 14. Behavior of lensing observable θ_∞ for REC no-horizon spacetime as a function of parameter b

$$\sum_{m=4}^{\infty} |\mu_{-m}| = \frac{u_{ps}^2 D_{OS}}{2\bar{p}\beta D_{OL}^2 D_{LS}} \frac{\exp\left(\frac{\bar{q}}{\bar{p}}\right) \left[\exp\left(\frac{8\pi}{\bar{p}}\right) + \exp\left(\frac{6\pi}{\bar{p}}\right) - 2\exp\left(\frac{\bar{q}}{\bar{p}}\right) \right]}{\exp\left(\frac{12\pi}{\bar{p}}\right) \left[\exp\left(\frac{4\pi}{\bar{p}}\right) - 1 \right]} \quad (50)$$

with μ_m and μ_{-m} being the fluxes of the m th image formed, respectively, from outside and inside of the photon sphere.

6. GRAVITATIONAL LENSING OBSERVABLES

We use REC spacetime to estimate the observables of massive dark objects in neighboring galaxies, particularly Sgr A*, M87*, NGC 4649, and NGC 1332, modeling them both as black holes as well as horizonless compact objects. A light ray traveling close to the photon sphere of a black hole or a horizonless compact object, depending on the impact parameter, passes around it once, twice, or many times before reaching an observer, creating a series of theoretically infinite number of relativistic images. We compute the angular positions as well as the separation and relative magnification of higher-order relativistic primary and secondary images, respectively, on the same and opposite sides of the source, taking $d = D_{LS}/D_{OS} = 0.5$.

When the spacetime is considered a black hole, we discover that an REC black hole with the same mass and distance has a smaller position in the innermost image (apparent radius of the photon sphere: θ_∞) than the Schwarzschild black hole spacetime and it further decreases with the higher values of b with $\theta_\infty \in (19.0178, 26.3299) \mu\text{as}$ for Sgr A* with a deviation of $7.3121 \mu\text{as}$ from the Schwarzschild black hole and for M87* $\in (14.2884, 19.782) \mu\text{as}$ with a deviation of $5.4936 \mu\text{as}$. Contrarily, the the angular separation between the outermost relativistic image

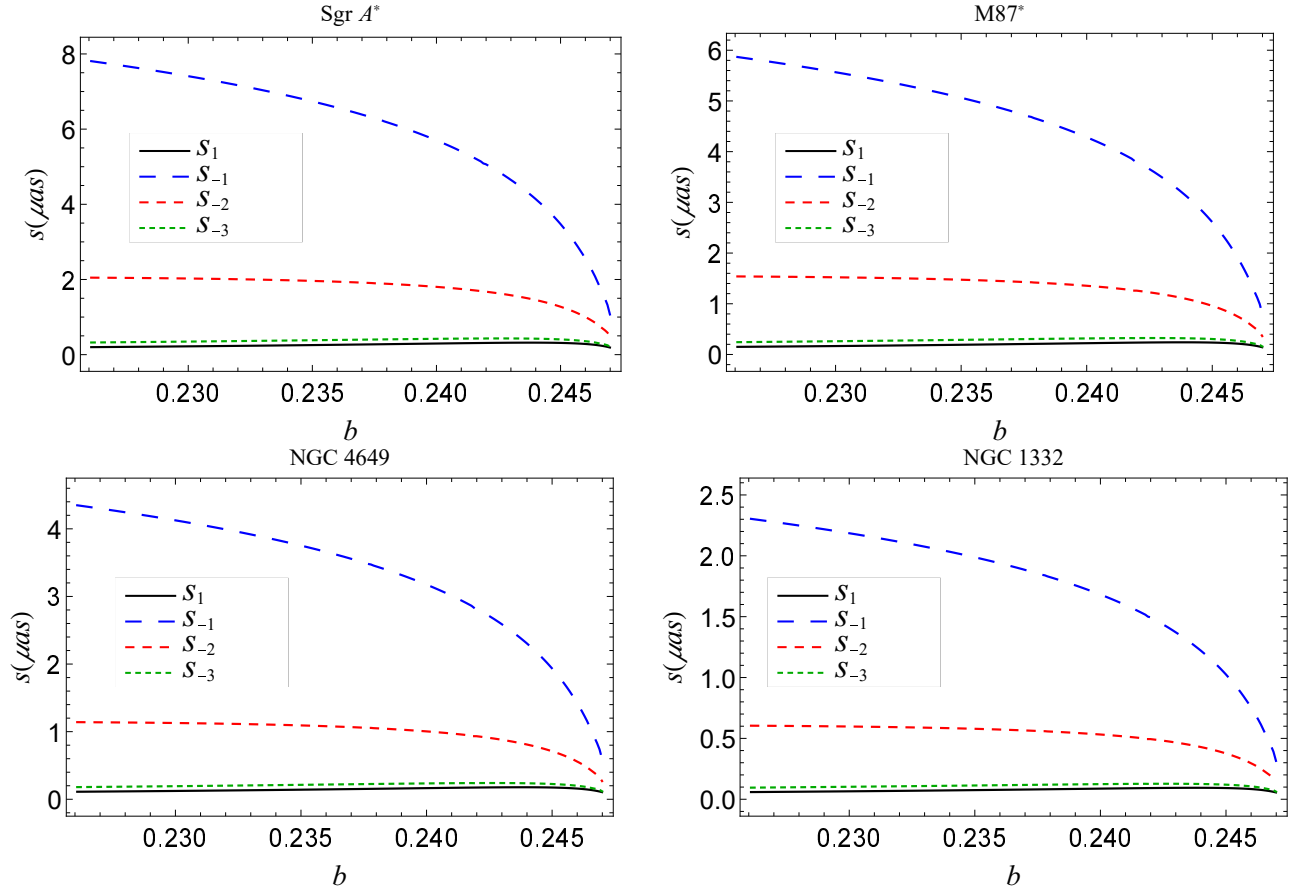


Figure 15. Behavior of lensing observables S_1 , S_{-1} , S_{-2} and S_{-3} for REC no-horizon spacetime as a function of parameter b .

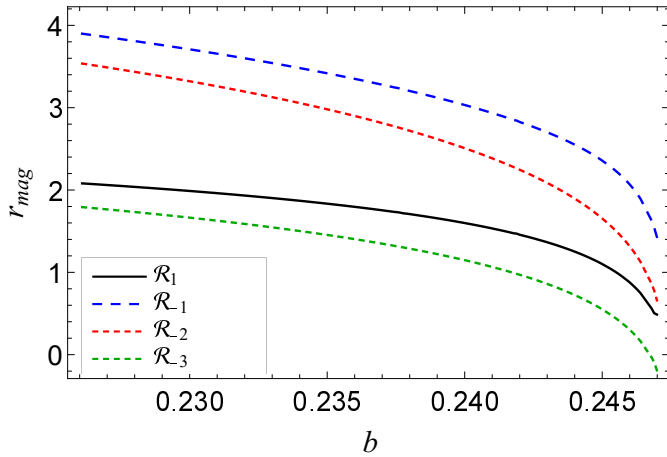


Figure 16. Behavior of strong lensing observables \mathcal{R}_1 , \mathcal{R}_{-1} , \mathcal{R}_{-2} and \mathcal{R}_{-3} for REC no-horizon spacetime as a function of parameter b .

and the others packaged at the photon sphere $\in (0.0329517, 0.199342) \mu\text{as}$ for Sgr A* and $\in (0.0247571, 0.149769) \mu\text{as}$ for M87*, with the separation s being five times greater than that for Schwarzschild black hole in both cases. In addition to being considerably faint, the spacing is well beyond

what is now possible with technology. Figure 8 depicts these typical observables, which comprises the position of the innermost image θ_∞ and the separation s , and are subsequently tabulated in Table 2. Moreover, we calculated the relative magnification of the outermost relativistic image caused by REC black hole spacetime gravitational lensing and discovered that the magnification decreases with parameter b (cf. Figure 10) and $\in (4.56657, 6.82188)$. The relative magnifications of first- and second-order images in REC black hole spacetime and Schwarzschild spacetime for different angular positions of the source using Eq. (31) are shown in Tables 4 and 5. We noticed that higher-order images are significantly demagnified, as expected. Considering the no-horizon REC spacetime, we discovered a series of relativistic images outside as well as inside the photon sphere, a feature that a black hole lacks. As depicted in Figure 14, θ_∞ decreases with increasing value of the parameter b , just as in the black hole situation and $\in (17.4462, 19.0178) \mu\text{as}$ for Sgr A* and $\in (13.1076, 14.2884) \mu\text{as}$ for M87*. Together with the image at θ_1 outside the photon sphere, we have taken into account the three additional images at θ_{-1} ,

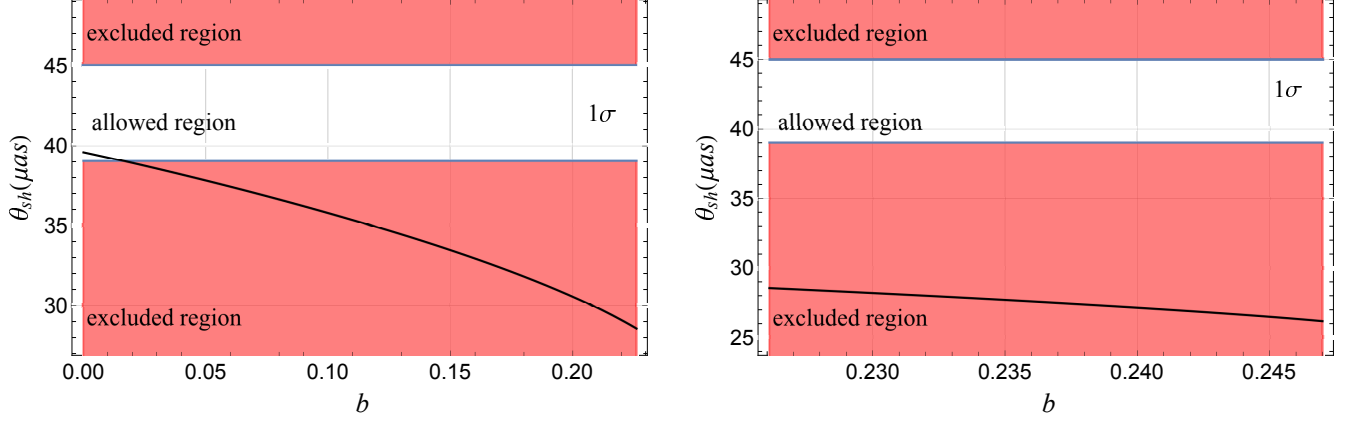


Figure 17. Shadow angular diameter $\theta_{\text{sh}} (= 2\theta_\infty)$ as a function of b , when M87* is modeled as REC spacetimes: (a) black hole (left) (b) no-horizon spacetime (right). The dark black line corresponds to calculated values of $2\theta_\infty$ as a function of b . The white/red regions represent areas that are 1σ consistent/inconsistent with the 2017 EHT observations, indicating that the latter imposed constraints on parameter b .

θ_{-2} , and θ_{-3} , which are well spaced with $s_1 \in (0.1882, 0.319045) \mu\text{as}$, $s_{-1} \in (1.12743, 7.8168) \mu\text{as}$, $s_{-2} \in (0.512824, 2.04872) \mu\text{as}$, and $s_{-3} \in (0.226226, 0.322697) \mu\text{as}$ for Sgr A* and $s_1 \in (0.141397, 0.239703) \mu\text{as}$, $s_{-1} \in (0.847053, 5.87288) \mu\text{as}$, $s_{-2} \in (0.385292, 1.53924) \mu\text{as}$, and $s_{-3} \in (0.169967, 0.242447) \mu\text{as}$ for M87* (see Figure 15). As we move from θ_1 or θ_{-1} toward θ_∞ , the angular separation between the consecutive images gets smaller. Further, the brightest images are those with a relative magnitude of \mathcal{R}_{-1} with $\mathcal{R}_{-1} \in (1.42485, 3.90258)$, $\mathcal{R}_{-2} \in (0.669416, 3.54039)$, $\mathcal{R}_{-3} \in (-0.17369, 1.79488)$, $\mathcal{R}_1 \in (0.42613, 2.0822)$ and brightness decreases in a similar way as separation as we go toward θ_∞ from θ_1 or θ_{-1} (see Figure 16). Similar to the black hole situation, the relative magnitude of the brightness of the images both inside and outside the photon sphere decreases with parameter b .

Finally, we gather updated data from 14 supermassive black holes whose masses and distances considerably vary in Table 3 in order to determine the time delays $\Delta T_{2,1}^s$ between first- and second-order relativistic primary images. The time delay $\Delta T_{2,1}^s$, for Sgr A*, M87*, NGC 4649, and NGC 1332, respectively, can reach ~ 8.8809 , ~ 12701.8 , ~ 9748.35 , and ~ 3036.03 minutes (see Table 3), with the deviation from the Schwarzschild black hole of same mass and distance being ~ 2.6159 , ~ 4677 , ~ 2871.35 , and ~ 894.26 minutes. As a result, the time delay in Sgr A* is much shorter for observation and much more difficult to measure. In the case of other black holes, the time delay $\Delta T_{2,1}^s$ can be in the hundreds of hours, which are adequate times for astronomical

measurements, provided we have sufficient angular resolution between two relativistic images.

7. CONSTRAINTS FROM EHT OBSERVATIONS OF M87* AND SGR A*

In 2019, black holes became a reality with the EHT Collaboration horizon-scale image of the supermassive black hole M87* (Akiyama et al. 2019a,b,c). Using a distance of $d = 16.8$ Mpc and their estimated mass of M87* $M = (6.5 \pm 0.7) \times 10^9 M_\odot$, the EHT Collaboration found a compact emission region size with angular diameter $\theta_d = 42 \pm 3 \mu\text{as}$ with the central flux depression with a factor of $\gtrsim 10$, which is the black hole shadow. Recently in 2022, the EHT observation also unveiled the image of supermassive black hole Sgr A* in our Milky Way showing a ring of diameter $\theta_d = 48.7 \pm 7 \mu\text{as}$, inferring a black hole mass of $M = 4.0_{-0.6}^{+1.1} \times 10^6 M_\odot$ and Schwarzschild shadow deviation $\delta = -0.08_{-0.09}^{+0.09}$ (VLTI), $-0.04_{-0.10}^{+0.09}$ (Keck). and provided us with yet another tool to investigate the nature of strong field gravity (Akiyama et al. 2022b,c,a). The EHT result for Sgr A* also only calculated the emission ring angular diameter $\theta_d = (51.8 \pm 2.3) \mu\text{as}$ with the prior perceived estimates M mentioned above and $D_{LS} = 8.15 \pm 0.15$ kpc (Akiyama et al. 2022a). The horizon-scale images of supermassive black holes furnish a theoretically fresh avenue for testing the theories of gravity and use the EHT results of the Sgr A* and M87* shadow size to infer constraints on the additional parameter of the underlying theory for a wide variety of black holes (Kumar et al. 2020d; Ghosh & Kumar 2020; Kumar & Ghosh 2020; Afrin et al. 2021; Kocherlakota et al. 2021; Akiyama et al. 2022a; Afrin & Ghosh 2022; Ghosh & Afrin 2022; Islam et al.

2022; Kumar Walia et al. 2022; Zakharov 2022) We use the EHT observation results of M87* and Sgr A* black hole shadows to constrain the deviation parameter b associated with REC black hole spacetime. By considering the apparent radius of the photon sphere θ_∞ as the angular size of the black hole shadow, we constrain the deviation parameter within the 1σ level. The EHT observational results are compatible with the reality of an event horizon, proving that it ruled out no-horizon spacetimes or naked singularities. However, we still model the M87* and Sgr A* as the REC spacetimes (both black holes and no horizon) and use the EHT observations results to test the viability of these REC spacetimes.

Constraints from M87:*—We find that the Schwarzschild black hole ($b = 0$) casts the largest shadow with its angular diameter $\theta_{\text{sh}} = 2\theta_\infty = 39.56069 \mu\text{as}$, which falls within the 1σ region for the black hole with mass $M = (6.5 \pm 0.7) \times 10^9 M_\odot$ and distance of $D_{\text{OL}} = 16.8$ Mpc (Akiyama et al. 2019a,b,c). Figure 17 depicts the angular diameter θ_{sh} as a function of b , with the black solid line corresponding to $\theta_{\text{sh}} = 39 \mu\text{as}$ for the REC black hole spacetime as M87*. The REC black hole spacetime metric when investigated with the EHT results of M87* within the 1σ bound, constrains parameter b , viz., $0 < b \leq 0.0165174$. Thus, based on Figure 17, within only a tiny part of parameter space, REC black hole spacetime could be a candidate for the astrophysical black holes. However, according to our results, the no-horizon spacetime does not agree with the EHT results of M87* (Figure 17).

Constraints from Sgr A:*—The EHT observation used three independent algorithms to find out that the averaged measured value of the shadow angular diameter, which lies in the range of $\theta_{\text{sh}} \in (46.9, 50) \mu\text{as}$, and the 1σ interval is $\in (41.7, 55.6) \mu\text{as}$ (Akiyama et al. 2022a). The angular diameter $\theta_{\text{sh}} \in (41.7, 55.6) \mu\text{as}$, which falls within the 1σ confidence region with the observed angular diameter of the EHT observation of Sgr A* black hole, strongly constrains the parameter $0.0 \leq b \leq 0.1881459$ for the REC black hole spacetime. Thus, within the finite parameter space, the REC black hole spacetime agrees with the EHT results of Sgr A* black hole shadow (see Figure 18). However, the REC no-horizon spacetimes are again inconsistent with the EHT observation of Sgr A*.

8. DISCUSSION AND CONCLUSION

General relativity’s no-hair theorem states that the Kerr-Newman metric (Newman et al. 1965) is the only stationary, axially symmetric, and asymptotically flat electro-vacuum solution of the Einstein equations (Israel 1967, 1968; Carter 1971; Hawking 1972; Robinson 1975). Three parameters describe it: mass, angular momentum, and electric charge. However, the third black hole parameter in the black hole, an electric charge, is often overlooked and implicitly set identically to zero. However, both classical and relativistic processes can lead to a small nonzero charge of black holes. Zero charges are a good approximation when dealing with neutral particles and photons. Even a small charge can significantly influence the motion of charged particles in the environs of black holes (Kumar et al. 2020d; Kumar & Ghosh 2021; Kumar et al. 2020c; Zhao & Xie 2016; Sotani & Miyamoto 2015). Therefore, one should not dump electric charge a priori in an astrophysical investigation. The gravitational effect of spacetime curvature by mass currents is the rotation of the plane of polarization for linearly polarized light rays, known as the Rytov effect (Rytov 1938). Such a gravitational rotation of the polarization plane in stationary spacetime is a gravitational analog of the electromagnetic Faraday effect (Piran et al. 1985; Ishihara et al. 1988; Nouri-Zonoz 1999).

Hence, we investigated the feasibility of comparing black holes from no-horizon spacetimes via strong gravitational lensing and analyzed the astrophysical consequences for several supermassive black holes considering electric charge. We look at a class of REC metrics, which are no-horizon spacetimes for parameters $b > b_E \approx 0.226$ and can also provide spherically symmetric black hole solutions when $0 < b \leq b_E$. Interestingly, we found that a photon sphere does exist for $0 < b \leq b_P \approx 0.247$ for REC spacetimes. On the other hand, the anti-photon sphere with stable circular orbits forms for no-horizon spacetime for $b_E < b \leq b_P$. We found that the radius of the photon sphere x_{ps} is a decreasing function of the b , while the opposite behavior is shown by the anti-photon sphere radius x_{aps} and they merge at $x \approx b_E$. The deflection angle α_D , for REC spacetime diverges at the critical impact parameter $u = u_{\text{ps}}$ and is a decreasing function of the impact parameter u as well as of the parameter b for REC black holes. Interestingly, for REC no-horizon spacetime in the limit $u \rightarrow u_{\text{ps}}^+$, the deflection angle α_D , increases rapidly in comparison when $u \rightarrow u_{\text{ps}}^-$ (cf. Figure 13). We modeled compact objects Sgr A*, M87* NGC 4649 and NGC 1332 as the REC spacetimes to evaluate the

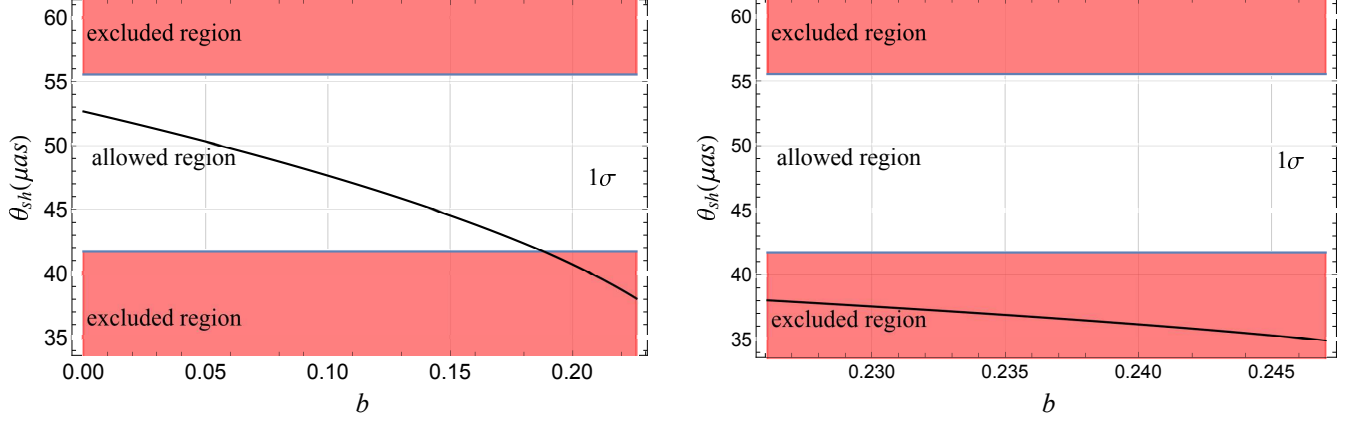


Figure 18. Shadow angular diameter $\theta_{\text{sh}} (= 2\theta_{\infty})$ as a function of b , when Sgr A* is modeled as REC spacetimes: (a) black hole (left) (b) no-horizon spacetime (right). The dark black line corresponds to calculated values of $2\theta_{\infty}$ as a function of b . The white/red regions represent areas that are 1σ consistent/inconsistent with the 2017 EHT observations, indicating that the latter imposed constraints on parameter b .

lensing observables, viz., angular positions of asymptotic relativistic images θ_{∞} , angular separations s , and relative magnifications r_{mag} of relativistic images. We found that θ_{∞} decreases with the parameter b for REC black holes as well as the for the no-horizon spacetime. $\theta_{\infty} \in (19.0178, 26.3299) \mu\text{as}$ for Sgr A* and $\in (14.2884, 19.782) \mu\text{as}$ for M87* when the compact objects are considered as REC black holes, while $\theta_{\infty} \in (17.4462, 19.0178) \mu\text{as}$ for Sgr A* and $\in (13.1076, 14.2884) \mu\text{as}$ for M87* when they are considered as REC no-horizon spacetimes. We have taken into account the three additional images apart from θ_1 , at angular positions θ_{-1} , θ_{-2} , and θ_{-3} for no-horizon spacetime. Further, we calculated the separation s for black hole spacetime and s_1, s_{-1}, s_{-2} and s_{-3} for REC no-horizon spacetime. The separation of the first relativistic image from the other packed images at θ_{∞} increases with b for $0 < b \leq b_E$. It further increases attaining a peak at $b \approx 0.224$ and thereafter decreases for $0.244 < b \leq b_P$. Contrarily, s_{-1}, s_{-2} and s_{-3} show a decreasing behavior with the parameter b . The separation s is much larger than that of Schwarzschild black hole for both Sgr A* and M87*, and is respectively, in the range 0.0329517-0.199342 and 0.0247571-0.149769 μas . On the other hand, $s_1 \in (0.1882, 0.319045) \mu\text{as}$, $s_{-1} \in (1.12743, 7.8168) \mu\text{as}$, $s_{-2} \in (0.512824, 2.04872) \mu\text{as}$, and $s_{-3} \in (0.226226, 0.322697) \mu\text{as}$ for Sgr A* and $s_1 \in (0.141397, 0.239703) \mu\text{as}$, $s_{-1} \in (0.847053, 5.87288) \mu\text{as}$, $s_{-2} \in (0.385292, 1.53924) \mu\text{as}$, and $s_{-3} \in (0.169967, 0.242447) \mu\text{as}$ for M87*. Consequently, the images formed from inside of the photon sphere are sufficiently separated from each other and some are marginally within the current resolution capability. Moreover, the relative magnification of the outermost

relativistic image caused by REC black hole spacetime decreases with b such that it varies between 4.56657 and 6.82188 orders of magnitude. On the contrary, $\mathcal{R}_1 \in (0.42613, 2.0822)$, $\mathcal{R}_{-1} \in (1.42485, 3.90258)$, $\mathcal{R}_{-2} \in (0.669416, 3.54039)$, $\mathcal{R}_{-3} \in (-0.17369, 1.79488)$. Thus, the observables of the images formed from inside the photon sphere are comparably different, showing that the strong gravitational lensing signature of no-horizon spacetime varies qualitatively from black holes.

We have also calculated the time delay $\Delta T_{2,1}^s$ between first- and second-order relativistic primary images for 22 supermassive black holes. Considering them as REC black hole spacetime, we found, e.g., $\Delta T_{2,1}^s$ for Sgr A*, M87*, NGC 4649, and NGC 1332, respectively, can reach ~ 8.8809 , ~ 12701.8 , ~ 9748.35 , and ~ 3036.03 minutes with the deviation from the Schwarzschild black hole of same mass and distance, respectively, being ~ 2.6159 , ~ 4677 , ~ 2871.35 , and ~ 894.26 minutes. Except for Sgr A*, the time delay can be in the hundreds of hours, which is adequate for astronomical measurements if we have enough angular resolution between two relativistic images.

On using the EHT results of the M87* and Sgr A* black hole shadows put a bound on the parameter b for the REC spacetime, which can be estimated based on the supposition that the relativistic image is the apparent size of the shadow at θ_{∞} . When investigated with the EHT results of M87* within the 1σ bound, the REC black hole spacetime metric puts a tight bound on the parameter b , viz., $0 < b \leq 0.0165174$. On the other hand, the results of Sgr A* restrict b such that $0.0 \leq b \leq 0.1881459$. Meanwhile, the REC no-horizon spacetimes are inconsistent with EHT observations of M87* and Sgr A*. Thus, EHT bounds

on θ_{sh} of Sgr A* and M87*, within the 1σ region, which place bounds on the parameter b , and hence we conclude that although the REC black holes agree with the EHT results in finite parameter space, the corresponding REC no-horizon spacetimes are complete ruled out. The spacetime under consideration is nonrotating; this work predicts strong deflection gravitational lensing signals for REC spacetime and hints at its no-horizon spacetimes.

Finally, due to the complicated REC spacetime metric, in the present analysis, we have limited our study to the spherically symmetric case, i.e., overlooked spin. It is because the silhouette of the shadow, as watched at infinity, has a shape that weakly

depends on the spin of the black hole (Bardeen 1973; Psaltis et al. 2020). However, we can anticipate our results on lensing by supermassive black holes Sgr A* and M87* are valid, and the EHT observation can also be assumed to test these spherical black holes. Meanwhile, a thorough analysis of the rotating counterpart will be a promising avenue for the future.

9. ACKNOWLEDGMENTS

J.K. would like to thank CSIR for providing SRF. S.U.I and S.G.G. would like to thank SERB-DST for the project No. CRG/2021/005771.

REFERENCES

- Afrin, M., & Ghosh, S. G. 2022, *Astrophys. J.*, 932, 51, doi: [10.3847/1538-4357/ac6dda](https://doi.org/10.3847/1538-4357/ac6dda)
- Afrin, M., Kumar, R., & Ghosh, S. G. 2021, *Mon. Not. Roy. Astron. Soc.*, 504, 5927, doi: [10.1093/mnras/stab1260](https://doi.org/10.1093/mnras/stab1260)
- Akiyama, K., et al. 2019a, *Astrophys. J. Lett.*, 875, L1, doi: [10.3847/2041-8213/ab0ec7](https://doi.org/10.3847/2041-8213/ab0ec7)
- . 2019b, *Astrophys. J. Lett.*, 875, L5, doi: [10.3847/2041-8213/ab0f43](https://doi.org/10.3847/2041-8213/ab0f43)
- . 2019c, *Astrophys. J. Lett.*, 875, L6, doi: [10.3847/2041-8213/ab1141](https://doi.org/10.3847/2041-8213/ab1141)
- . 2022a, *Astrophys. J. Lett.*, 930, L17, doi: [10.3847/2041-8213/ac6756](https://doi.org/10.3847/2041-8213/ac6756)
- . 2022b, *Astrophys. J. Lett.*, 930, L12, doi: [10.3847/2041-8213/ac6674](https://doi.org/10.3847/2041-8213/ac6674)
- . 2022c, *Astrophys. J. Lett.*, 930, L16, doi: [10.3847/2041-8213/ac6672](https://doi.org/10.3847/2041-8213/ac6672)
- Ali, M. S., & Ghosh, S. G. 2018, *Phys. Rev. D*, 98, 084025, doi: [10.1103/PhysRevD.98.084025](https://doi.org/10.1103/PhysRevD.98.084025)
- . 2019, *Phys. Rev. D*, 99, 024015, doi: [10.1103/PhysRevD.99.024015](https://doi.org/10.1103/PhysRevD.99.024015)
- Ansoldi, S. 2008, in *Conference on Black Holes and Naked Singularities*. <https://arxiv.org/abs/0802.0330>
- Ayon-Beato, E., & Garcia, A. 1998, *Phys. Rev. Lett.*, 80, 5056, doi: [10.1103/PhysRevLett.80.5056](https://doi.org/10.1103/PhysRevLett.80.5056)
- . 1999, *Gen. Rel. Grav.*, 31, 629, doi: [10.1023/A:1026640911319](https://doi.org/10.1023/A:1026640911319)
- Bambi, C. 2014, *Phys. Lett. B*, 730, 59, doi: [10.1016/j.physletb.2014.01.037](https://doi.org/10.1016/j.physletb.2014.01.037)
- Bardeen, J. M. 1968, in *Proc. Int. Conf. GR5, Tbilisi*, Vol. 174, 174
- Bardeen, J. M. 1973, in *Les Houches Summer School of Theoretical Physics: Black Holes*, 215–240
- Borde, A. 1994, *Phys. Rev. D*, 50, 3692, doi: [10.1103/PhysRevD.50.3692](https://doi.org/10.1103/PhysRevD.50.3692)
- . 1997, *Phys. Rev. D*, 55, 7615, doi: [10.1103/PhysRevD.55.7615](https://doi.org/10.1103/PhysRevD.55.7615)
- Bozza, V. 2002, *Phys. Rev. D*, 66, 103001, doi: [10.1103/PhysRevD.66.103001](https://doi.org/10.1103/PhysRevD.66.103001)
- . 2003, *Phys. Rev. D*, 67, 103006, doi: [10.1103/PhysRevD.67.103006](https://doi.org/10.1103/PhysRevD.67.103006)
- . 2015, *AIP Conf. Proc.*, 1577, 89, doi: [10.1063/1.4861946](https://doi.org/10.1063/1.4861946)
- Bozza, V., Capozziello, S., Iovane, G., & Scarpetta, G. 2001, *Gen. Rel. Grav.*, 33, 1535, doi: [10.1023/A:1012292927358](https://doi.org/10.1023/A:1012292927358)
- Bozza, V., & Mancini, L. 2004a, *Astrophys. J.*, 611, 1045, doi: [10.1086/422309](https://doi.org/10.1086/422309)
- . 2004b, *Gen. Rel. Grav.*, 36, 435, doi: [10.1023/B:GERG.0000010486.58026.4f](https://doi.org/10.1023/B:GERG.0000010486.58026.4f)
- Breton, N., & Lopez, L. A. 2016, *Phys. Rev. D*, 94, 104008, doi: [10.1103/PhysRevD.94.104008](https://doi.org/10.1103/PhysRevD.94.104008)
- Bronnikov, K. A. 2000, *Phys. Rev. Lett.*, 85, 4641, doi: [10.1103/PhysRevLett.85.4641](https://doi.org/10.1103/PhysRevLett.85.4641)
- . 2001, *Phys. Rev. D*, 63, 044005, doi: [10.1103/PhysRevD.63.044005](https://doi.org/10.1103/PhysRevD.63.044005)
- . 2017, *Phys. Rev. D*, 96, 128501, doi: [10.1103/PhysRevD.96.128501](https://doi.org/10.1103/PhysRevD.96.128501)
- Bronnikov, K. A., & Fabris, J. C. 2006, *Phys. Rev. Lett.*, 96, 251101, doi: [10.1103/PhysRevLett.96.251101](https://doi.org/10.1103/PhysRevLett.96.251101)
- Burinskii, A., & Hildebrandt, S. R. 2002, *Phys. Rev. D*, 65, 104017, doi: [10.1103/PhysRevD.65.104017](https://doi.org/10.1103/PhysRevD.65.104017)
- Capozziello, S., Lambiase, G., Papini, G., & Scarpetta, G. 1999, *Phys. Lett. A*, 254, 11, doi: [10.1016/S0375-9601\(99\)00121-8](https://doi.org/10.1016/S0375-9601(99)00121-8)
- Capozziello, S., & Re, V. 2001, *Phys. Lett. A*, 290, 115, doi: [10.1016/S0375-9601\(01\)00671-5](https://doi.org/10.1016/S0375-9601(01)00671-5)
- Carter, B. 1971, *Phys. Rev. Lett.*, 26, 331, doi: [10.1103/PhysRevLett.26.331](https://doi.org/10.1103/PhysRevLett.26.331)

- Chen, S.-b., & Jing, J.-l. 2009, *Phys. Rev. D*, 80, 024036, doi: [10.1103/PhysRevD.80.024036](https://doi.org/10.1103/PhysRevD.80.024036)
- Clarke, C. J. S. 1994, *Classical and Quantum Gravity*, 11, 1375, doi: [10.1088/0264-9381/11/6/003](https://doi.org/10.1088/0264-9381/11/6/003)
- Darwin, C. 1959, *Proceedings of the Royal Society of London Series A*, 249, 180, doi: <https://doi.org/10.1098/rspa.1959.0015>
- Dey, S., & Chakrabarti, S. 2019, *Eur. Phys. J. C*, 79, 504, doi: [10.1140/epjc/s10052-019-7004-0](https://doi.org/10.1140/epjc/s10052-019-7004-0)
- Dymnikova, I. 1992, *Gen. Rel. Grav.*, 24, 235, doi: [10.1007/BF00760226](https://doi.org/10.1007/BF00760226)
- . 2004, *Class. Quant. Grav.*, 21, 4417, doi: [10.1088/0264-9381/21/18/009](https://doi.org/10.1088/0264-9381/21/18/009)
- Eiroa, E. F., & Romero, G. E. 2008, *Phys. Lett. B*, 663, 377, doi: [10.1016/j.physletb.2008.04.016](https://doi.org/10.1016/j.physletb.2008.04.016)
- Eiroa, E. F., Romero, G. E., & Torres, D. F. 2002, *Phys. Rev. D*, 66, 024010, doi: [10.1103/PhysRevD.66.024010](https://doi.org/10.1103/PhysRevD.66.024010)
- Fan, Z.-Y., & Wang, X. 2016, *Phys. Rev. D*, 94, 124027, doi: [10.1103/PhysRevD.94.124027](https://doi.org/10.1103/PhysRevD.94.124027)
- Fernando, S., & Correa, J. 2012, *Phys. Rev. D*, 86, 064039, doi: [10.1103/PhysRevD.86.064039](https://doi.org/10.1103/PhysRevD.86.064039)
- Fernando, S., & Roberts, S. 2002, *Gen. Rel. Grav.*, 34, 1221, doi: [10.1023/A:1019726501344](https://doi.org/10.1023/A:1019726501344)
- Flachi, A., & Lemos, J. P. S. 2013, *Phys. Rev. D*, 87, 024034, doi: [10.1103/PhysRevD.87.024034](https://doi.org/10.1103/PhysRevD.87.024034)
- Frittelli, S., Kling, T. P., & Newman, E. T. 2000, *Phys. Rev. D*, 61, 064021, doi: [10.1103/PhysRevD.61.064021](https://doi.org/10.1103/PhysRevD.61.064021)
- Ghosh, S. G., & Afrin, M. 2022, <https://arxiv.org/abs/2206.02488>
- Ghosh, S. G., & Amir, M. 2015, *Eur. Phys. J. C*, 75, 553, doi: [10.1140/epjc/s10052-015-3786-x](https://doi.org/10.1140/epjc/s10052-015-3786-x)
- Ghosh, S. G., & Kothawala, D. 2008, *Gen. Rel. Grav.*, 40, 9, doi: [10.1007/s10714-007-0511-6](https://doi.org/10.1007/s10714-007-0511-6)
- Ghosh, S. G., Kumar, A., & Singh, D. V. 2020, *Phys. Dark Univ.*, 30, 100660, doi: [10.1016/j.dark.2020.100660](https://doi.org/10.1016/j.dark.2020.100660)
- Ghosh, S. G., & Kumar, R. 2020, *Class. Quant. Grav.*, 37, 245008, doi: [10.1088/1361-6382/abc134](https://doi.org/10.1088/1361-6382/abc134)
- Ghosh, S. G., Kumar, R., & Islam, S. U. 2021, *JCAP*, 03, 056, doi: [10.1088/1475-7516/2021/03/056](https://doi.org/10.1088/1475-7516/2021/03/056)
- Gliner, E. B. 1966, *Soviet Journal of Experimental and Theoretical Physics*, 22, 378
- Gyulchev, G., & Yazadjiev, S. 2007, *AIP Conf. Proc.*, 946, 106, doi: [10.1063/1.2806045](https://doi.org/10.1063/1.2806045)
- Gyulchev, G. N., & Yazadjiev, S. S. 2008, *Phys. Rev. D*, 78, 083004, doi: [10.1103/PhysRevD.78.083004](https://doi.org/10.1103/PhysRevD.78.083004)
- Harada, T. 2004, *Pramana*, 63, 741, doi: [10.1007/BF02705196](https://doi.org/10.1007/BF02705196)
- Hawking, S. W. 1972, *Commun. Math. Phys.*, 25, 152, doi: [10.1007/BF01877517](https://doi.org/10.1007/BF01877517)
- Hawking, S. W., & Ellis, G. F. R. 2011, *The Large Scale Structure of Space-Time*, Cambridge Monographs on Mathematical Physics (Cambridge University Press), doi: [10.1017/CBO9780511524646](https://doi.org/10.1017/CBO9780511524646)
- Hayward, S. A. 2006, *Phys. Rev. Lett.*, 96, 031103, doi: [10.1103/PhysRevLett.96.031103](https://doi.org/10.1103/PhysRevLett.96.031103)
- Ishihara, H., Takahashi, M., & Tomimatsu, A. 1988, *Phys. Rev. D*, 38, 472, doi: [10.1103/PhysRevD.38.472](https://doi.org/10.1103/PhysRevD.38.472)
- Islam, S. U., & Ghosh, S. G. 2021, *Phys. Rev. D*, 103, 124052, doi: [10.1103/PhysRevD.103.124052](https://doi.org/10.1103/PhysRevD.103.124052)
- Islam, S. U., Ghosh, S. G., & Maharaj, S. D. 2022, <https://arxiv.org/abs/2203.00957>
- Islam, S. U., Kumar, J., & Ghosh, S. G. 2021, *JCAP*, 10, 013, doi: [10.1088/1475-7516/2021/10/013](https://doi.org/10.1088/1475-7516/2021/10/013)
- Islam, S. U., Kumar, R., & Ghosh, S. G. 2020, *JCAP*, 09, 030, doi: [10.1088/1475-7516/2020/09/030](https://doi.org/10.1088/1475-7516/2020/09/030)
- Israel, W. 1967, *Phys. Rev.*, 164, 1776, doi: [10.1103/PhysRev.164.1776](https://doi.org/10.1103/PhysRev.164.1776)
- . 1968, *Commun. Math. Phys.*, 8, 245, doi: [10.1007/BF01645859](https://doi.org/10.1007/BF01645859)
- Joshi, P. S. 1993, *Int. Ser. Monogr. Phys.*, 87
- Joshi, P. S., ed. 2012, *Gravitational Collapse and Spacetime Singularities*, Cambridge Monographs on Mathematical Physics (Cambridge University Press), doi: [10.1017/CBO9780511536274](https://doi.org/10.1017/CBO9780511536274)
- Junior, E. L. B., Rodrigues, M. E., & Houndjo, M. J. S. 2015, *JCAP*, 10, 060, doi: [10.1088/1475-7516/2015/10/060](https://doi.org/10.1088/1475-7516/2015/10/060)
- Karouzos, M. 2018, *Nature Astronomy*, 2, 764, doi: [10.1038/s41550-018-0588-8](https://doi.org/10.1038/s41550-018-0588-8)
- Kocherlakota, P., et al. 2021, *Phys. Rev. D*, 103, 104047, doi: [10.1103/PhysRevD.103.104047](https://doi.org/10.1103/PhysRevD.103.104047)
- Kothawala, D., & Ghosh, S. G. 2004, *Phys. Rev. D*, 70, 104010, doi: [10.1103/PhysRevD.70.104010](https://doi.org/10.1103/PhysRevD.70.104010)
- Kumar, A., Ghosh, S. G., & Maharaj, S. D. 2020a, *Phys. Dark Univ.*, 30, 100634, doi: [10.1016/j.dark.2020.100634](https://doi.org/10.1016/j.dark.2020.100634)
- Kumar, A., Singh, D. V., & Ghosh, S. G. 2020b, *Annals Phys.*, 419, 168214, doi: [10.1016/j.aop.2020.168214](https://doi.org/10.1016/j.aop.2020.168214)
- Kumar, A., Veer Singh, D., & Ghosh, S. G. 2019, *Eur. Phys. J. C*, 79, 275, doi: [10.1140/epjc/s10052-019-6773-9](https://doi.org/10.1140/epjc/s10052-019-6773-9)
- Kumar, A., Walia, R. K., & Ghosh, S. G. 2022a, *Universe*, 8, 232, doi: [10.3390/universe8040232](https://doi.org/10.3390/universe8040232)
- Kumar, J., Islam, S. U., & Ghosh, S. G. 2022b, *Eur. Phys. J. C*, 82, 443, doi: [10.1140/epjc/s10052-022-10357-2](https://doi.org/10.1140/epjc/s10052-022-10357-2)
- Kumar, R., & Ghosh, S. G. 2020, *Astrophys. J.*, 892, 78, doi: [10.3847/1538-4357/ab77b0](https://doi.org/10.3847/1538-4357/ab77b0)
- . 2021, *Class. Quant. Grav.*, 38, 8, doi: [10.1088/1361-6382/abdd48](https://doi.org/10.1088/1361-6382/abdd48)
- Kumar, R., Islam, S. U., & Ghosh, S. G. 2020c, *Eur. Phys. J. C*, 80, 1128, doi: [10.1140/epjc/s10052-020-08606-3](https://doi.org/10.1140/epjc/s10052-020-08606-3)

- Kumar, R., Kumar, A., & Ghosh, S. G. 2020d, *Astrophys. J.*, 896, 89, doi: [10.3847/1538-4357/ab8c4a](https://doi.org/10.3847/1538-4357/ab8c4a)
- Kumar Walia, R., Ghosh, S. G., & Maharaj, S. D. 2022. <https://arxiv.org/abs/2207.00078>
- Lemos, J. P. S., & Zanchin, V. T. 2011, *Phys. Rev. D*, 83, 124005, doi: [10.1103/PhysRevD.83.124005](https://doi.org/10.1103/PhysRevD.83.124005)
- Luminet, J. P. 1979, *A&A*, 75, 228
- Majumdar, A. S., & Mukherjee, N. 2005, *Mod. Phys. Lett. A*, 20, 2487, doi: [10.1142/S0217732305017676](https://doi.org/10.1142/S0217732305017676)
- Newman, E. T., Couch, R., Chinnapared, K., et al. 1965, *J. Math. Phys.*, 6, 918, doi: [10.1063/1.1704351](https://doi.org/10.1063/1.1704351)
- Nouri-Zonoz, M. 1999, *Phys. Rev. D*, 60, 024013, doi: [10.1103/PhysRevD.60.024013](https://doi.org/10.1103/PhysRevD.60.024013)
- Penrose, R. 1969, *Riv. Nuovo Cim.*, 1, 252, doi: [10.1023/A:1016578408204](https://doi.org/10.1023/A:1016578408204)
- Perlick, V. 2004, *Phys. Rev. D*, 69, 064017, doi: [10.1103/PhysRevD.69.064017](https://doi.org/10.1103/PhysRevD.69.064017)
- Piran, T., Safer, P. N., & Stark, R. F. 1985, *Phys. Rev. D*, 32, 3101, doi: [10.1103/PhysRevD.32.3101](https://doi.org/10.1103/PhysRevD.32.3101)
- Psaltis, D., et al. 2020, *Phys. Rev. Lett.*, 125, 141104, doi: [10.1103/PhysRevLett.125.141104](https://doi.org/10.1103/PhysRevLett.125.141104)
- Robinson, D. C. 1975, *Phys. Rev. Lett.*, 34, 905, doi: [10.1103/PhysRevLett.34.905](https://doi.org/10.1103/PhysRevLett.34.905)
- Rodrigues, M. E., & Silva, M. V. d. S. 2018, *JCAP*, 06, 025, doi: [10.1088/1475-7516/2018/06/025](https://doi.org/10.1088/1475-7516/2018/06/025)
- Rytov, S. M. 1938, in *Dokl. Akad. Nauk SSSR*, 263–266
- Sahu, S., Lochan, K., & Narasimha, D. 2015, *Phys. Rev. D*, 91, 063001, doi: [10.1103/PhysRevD.91.063001](https://doi.org/10.1103/PhysRevD.91.063001)
- Sajadi, S. N., & Riazi, N. 2017, *Gen. Rel. Grav.*, 49, 45, doi: [10.1007/s10714-017-2209-8](https://doi.org/10.1007/s10714-017-2209-8)
- Sakharov, A. D. 1966, *Soviet Journal of Experimental and Theoretical Physics*, 22, 241
- Saleh, M., Thomas, B. B., & Kofane, T. C. 2018, *Eur. Phys. J. C*, 78, 325, doi: [10.1140/epjc/s10052-018-5818-9](https://doi.org/10.1140/epjc/s10052-018-5818-9)
- Schee, J., & Stuchlik, Z. 2015, *JCAP*, 06, 048, doi: [10.1088/1475-7516/2015/06/048](https://doi.org/10.1088/1475-7516/2015/06/048)
- Shaikh, R., Banerjee, P., Paul, S., & Sarkar, T. 2019, *Phys. Rev. D*, 99, 104040, doi: [10.1103/PhysRevD.99.104040](https://doi.org/10.1103/PhysRevD.99.104040)
- Sharif, M., & Javed, W. 2011, *Can. J. Phys.*, 89, 1027, doi: [10.1139/p11-089](https://doi.org/10.1139/p11-089)
- Singh, D. V., Ghosh, S. G., & Maharaj, S. D. 2020, *Annals Phys.*, 412, 168025, doi: [10.1016/j.aop.2019.168025](https://doi.org/10.1016/j.aop.2019.168025)
- Singh, T. P. 1999, *J. Astrophys. Astron.*, 20, 221, doi: [10.1007/BF02702354](https://doi.org/10.1007/BF02702354)
- Sotani, H., & Miyamoto, U. 2015, *Phys. Rev. D*, 92, 044052, doi: [10.1103/PhysRevD.92.044052](https://doi.org/10.1103/PhysRevD.92.044052)
- Takahashi, R. 2005, *Publ. Astron. Soc. Jap.*, 57, 273, doi: [10.1093/pasj/57.2.273](https://doi.org/10.1093/pasj/57.2.273)
- Toshmatov, B., Stuchlík, Z., & Ahmedov, B. 2018, *Phys. Rev. D*, 98, 028501, doi: [10.1103/PhysRevD.98.028501](https://doi.org/10.1103/PhysRevD.98.028501)
- Toshmatov, B., Stuchlík, Z., Ahmedov, B., & Malafarina, D. 2019, *Phys. Rev. D*, 99, 064043, doi: [10.1103/PhysRevD.99.064043](https://doi.org/10.1103/PhysRevD.99.064043)
- Ulhoa, S. C. 2014, *Braz. J. Phys.*, 44, 380, doi: [10.1007/s13538-014-0209-7](https://doi.org/10.1007/s13538-014-0209-7)
- Virbhadra, K. S. 1996. <https://arxiv.org/abs/gr-qc/9606004>
- . 1999, *Phys. Rev. D*, 60, 104041, doi: [10.1103/PhysRevD.60.104041](https://doi.org/10.1103/PhysRevD.60.104041)
- . 2009, *Phys. Rev. D*, 79, 083004, doi: [10.1103/PhysRevD.79.083004](https://doi.org/10.1103/PhysRevD.79.083004)
- Virbhadra, K. S., & Ellis, G. F. R. 2000, *Phys. Rev. D*, 62, 084003, doi: [10.1103/PhysRevD.62.084003](https://doi.org/10.1103/PhysRevD.62.084003)
- . 2002, *Phys. Rev. D*, 65, 103004, doi: [10.1103/PhysRevD.65.103004](https://doi.org/10.1103/PhysRevD.65.103004)
- Virbhadra, K. S., & Keeton, C. R. 2008, *Phys. Rev. D*, 77, 124014, doi: [10.1103/PhysRevD.77.124014](https://doi.org/10.1103/PhysRevD.77.124014)
- Virbhadra, K. S., Narasimha, D., & Chitre, S. M. 1998, *Astron. Astrophys.*, 337, 1. <https://arxiv.org/abs/astro-ph/9801174>
- Wald, R. M. 1997, 69, doi: [10.1007/978-94-017-0934-7_5](https://doi.org/10.1007/978-94-017-0934-7_5)
- Wheeler, J. A. 1963, *Relativity, Groups and Topology* (New York: Gordon and Breach)
- Zajaček, M., Tursunov, A., Eckart, A., & Britzen, S. 2018, *Mon. Not. Roy. Astron. Soc.*, 480, 4408, doi: [10.1093/mnras/sty2182](https://doi.org/10.1093/mnras/sty2182)
- Zakharov, A. F. 2022, *Universe*, 8, 141, doi: [10.3390/universe8030141](https://doi.org/10.3390/universe8030141)
- Zaslavskii, O. B. 2009, *Phys. Rev. D*, 80, 064034, doi: [10.1103/PhysRevD.80.064034](https://doi.org/10.1103/PhysRevD.80.064034)
- Zhao, S.-S., & Xie, Y. 2016, *JCAP*, 07, 007, doi: [10.1088/1475-7516/2016/07/007](https://doi.org/10.1088/1475-7516/2016/07/007)